



ΕΘΝΙΚΟ ΜΕΤΣΟΒΙΟ ΠΟΛΥΤΕΧΝΕΙΟ
ΣΧΟΛΗ ΗΛΕΚΤΡΟΛΟΓΩΝ ΜΗΧΑΝΙΚΩΝ ΚΑΙ
ΜΗΧΑΝΙΚΩΝ ΥΠΟΛΟΓΙΣΤΩΝ

ΤΟΜΕΑΣ ΗΛΕΚΤΡΙΚΩΝ ΒΙΟΜΗΧΑΝΙΚΩΝ ΔΙΑΤΑΞΕΩΝ

Διπλωματική Εργασία

Ανεμογεννητριες σε συστήματα παραγωγής ηλεκτρικής ενέργειας .

Όνοματεπώνυμο: MOUSSA DORY

Όνομα Πατρός: NICOLAS

Αριθμός Μητρώου: 03104632

Επιβλέπων: μαρια-παρασκευη ιωαννιδου

Καθηγητρια ΕΜΠ

ΑΘΗΝΑ

27/06/2011



ΕΘΝΙΚΟ ΜΕΤΣΟΒΙΟ ΠΟΛΥΤΕΧΝΕΙΟ
ΣΧΟΛΗ ΗΛΕΚΤΡΟΛΟΓΩΝ ΜΗΧΑΝΙΚΩΝ ΚΑΙ
ΜΗΧΑΝΙΚΩΝ ΥΠΟΛΟΓΙΣΤΩΝ

ΤΟΜΕΑΣ ΗΛΕΚΤΡΙΚΩΝ ΒΙΟΜΗΧΑΝΙΚΩΝ ΔΙΑΤΑΞΕΩΝ

Διπλωματική Εργασία

Ανεμογεννητριες σε συστήματα παραγωγής ηλεκτρικής ενέργειας .

Όνοματεπώνυμο: MOUSSA DORY

Όνομα Πατρός: NICOLAS

Αριθμός Μητρώου: 03104632

Επιβλέπων: μαρια-παρασκευη ιωαννιδου

Καθηγητρια ΕΜΠ

ΑΘΗΝΑ

27/06/2011

Copyright © MOUSSA DORY

All rights reserved Με επιφύλαξη παντός δικαιώματος

Απαγορεύεται η αντιγραφή , αποθήκευση και αναδιανομή της παρούσας εργασίας , εξ ολοκλήρου ή τμήματος αυτής για εμπορικούς σκοπούς. Επιτρέπεται η αντιγραφή , αποθήκευση και διανομή για σκοπό μη κερδοσκοπικό , ερευνητικό ή εκπαιδευτικό , με την προϋπόθεση όμως να διατηρείται το παρόν μήνυμα και να αναφέρεται η πηγή προέλευσης. Οι απόψεις και τα συμπεράσματα που περιέχονται στην παρούσα εργασία εκφράζουν τον συγγραφέα και δεν αποτελούν επίσημες θέσεις του Εθνικού Μετσόβιου Πολυτεχνείου.

FORWARD

This thesis presents a general background on utility-scale wind power, providing the interested reader with a basis for understanding wind power in general, as well as providing a solid foundation for further understanding of the technical, economic, and policy dimensions of wind power development world-wide. The concepts in this thesis are illustrated with economic data and current policy from the U.S. wind sector. The paper provides extensive references and links to well-established bodies of knowledge on wind power in written form and on the Web, enabling the reader to become aware of and conversant in the latest developments in wind power for clean energy generation.

KEY WORDS

Offshore wind energy technology , wind turbine , double output induction generator
environmental impacts of wind energy farms

Table of contents

Introduction.....	11
1 Benefits of Wind Power.....	11
2 Wind Turbines and Wind Parks.....	12
3 Tower Height.....	12
4 History of Offshore Wind.....	13
5 Offshore Wind Resources.....	13
6 Environmental benefits.....	14
7 economics.....	14
8 Cost Measures.....	14
9 Economics of Offshore Wind.....	15

Chapter 1

Review Of Knowledge Development For The Design Of Offshore Wind Energy Technology

1.1 Design methodological knowledge.....	17
1.2 Design with a narrow scope.....	17
1.3 Integration of disciplines.....	18
1.4 The appropriate perspective.....	19

Chapter 2

Hybrid Configuration of Darrieus And Savonius Rotors for Stand-Alone Wind Turbine-Generator Systemes

2.1 Introduction	20
2.2 The Derries Savona’s hybrid turbine.....	20
2.3 A wind turbine-generator system for a stand-alone power source.....	21
2.3.1 Outline of a stand-alone wind turbine-generator system.....	21
2.3.2 Control method for system operation.....	21
2.3.3 Evaluation of the dynamic behaviour of the system.....	22
2.3.4 Starting characteristics.....	22
2.3.5 Behaviour under load control.....	22

CHAPTER 3

Design And Control

3.1 Introduction.....	23
3.2 Blade bending dynamics.....	23
3.3 Derivation of three-mass model.....	24
3.4 Variable speed variable pitch wind.....	25
3.5 Non-linear control methods.....	25
3.6 Modelling and control Design.....	28
3.6.1 Modelling.....	29
3.6.1.1 Non-linear model.....	29
3.6.1.2 Linear mode.....	30
3.7 Gain scheduled proportional integral controller.....	30

3.8 Linear quadratic regulator (LQR).....	30
3.9 Control design	30
3.10 Conclusion.....	32

Chapter 4

The System Design Process

4.1 Efficiency of the Search for Solutions.....	33
4.2 Regions of operation and linear models.....	37

Chapter5

Sliding Mode Control For Efficiency Optimization Of Wind Energy Systems With Double Output Induction Generator

5.1 Introduction	45
5.2 Modelling of the DOIG with slip power recovery	46
5.3 Conclusion.....	51

CHAPTER 6

Simulating Dynamic Stall in a Two-Dimensional Vertical-Axis wind turbine (VAWT)

6.1 Introduction	51
------------------------	----

6.2 Motion and aerodynamics of A VAWT.....	53
6.3 Simulation definition.....	55
6.3.1 Model geometry.....	55
6.3.2 Computational space grid.....	56
6.3.3 Simulated flow conditions.....	57
6.4 Validation of the results of different turbulence models	57
6.4.1 URANS models (unsteady Reynolds-averaged Navier–Stokes).....	60
6.4.2 LES (large eddy simulation).....	61
6.4.3 DES (detached eddy simulation).....	61
6.5 Comparison of force simulation.....	61
6.6 Verification of grid sensitivity	62
6.6.1 Time step refinement.....	62
6.6.2 Space grid refinement.....	62
6.7 Verifying high- frequency variation in force.....	63
6.8 Conclusion	65

CHAPTER 7

Environmental Impacts Of Wind Energy Farms

7.1 Impacts on human health and well-being	67
7.2 Noise.....	67
7.2.1 Noise levels.....	69
7.2.2 Mitigation measures	69
7.3 Shadow flicker.....	69
7.3.1 Impacts.....	69
7.3.2 Mitigation measures.....	70
7.4 Wind turbines and bird populations.....	70

7.5 Can wind turbines interfere with television reception?.....	70
7.6 What happens when a turbine finishes its life?.....	71

Chapter 8

Onshore And Offshore Wind Farms Relative Comparison

8.1 Onshore vs offshore wind turbines.....	72
8.2 Onshore.....	72
8.3 Offshore.....	72
8.4 Typical support structures of offshore wind turbines.....	73
8.4.1 Gravity structures.....	73
8.4.2 Monopile.....	73
8.4.3 Guyed monopile towers.....	73
8.4.4 Tripods.....	74
8.4.5 Braced lattice frame.....	74
8.4.6 Suction buckets.....	74
8.5 Typical foundations	74
8.5.1 Gravity caissons.....	74
8.5.2 Driven pipe pile.....	75
8.5.3 Post-grouted closed-end pile in predrilled hole.	75
8.5.4 Drilled shafts or bored, Cast-in-Place Concrete Pile.....	75
8.5.5 Composite “Drive-Drill-Drive” Pile.....	75
8.5.6 Suction caissons.....	75
8.6 Conclusions.....	76

Introduction

Over 15,000 billion kWh of electricity are generated annually worldwide. Of this, about 65% is produced by burning fossil fuels and the remainder is obtained from other sources, including nuclear, hydropower, geothermal, biomass, solar and wind energy. Only about 0.3% of this power is produced by converting the kinetic energy in the wind into electrical energy. However, the use of wind for electricity generation has been expanding rapidly in recent years, due largely to technological improvements, industry maturation and an increasing concern with the emissions associated with burning fossil fuels. There is still more room to grow, as only a small portion of the useable wind resource is being tapped. Government and electrical industry regulations, as well as government incentives, play a large role in determining how quickly wind power is adopted. Effective policies will help level the playing field and ensure that wind can compete fairly with other fuel sources in the electricity market.

1 Benefits of wind power

Wind power has many benefits that make it an attractive source of power for both utility-scale and small, distributed power generation applications. The beneficial characteristics of wind power include:

- Clean and inexhaustible fuel—Wind power produces no emissions and is not depleted over time. A single one megawatt (1 MW) wind turbine running for one year can displace over 1,500 tons of carbon dioxide, 6.5 tons of sulfur dioxide, 3.2 tons of nitrogen oxides, and 60 pounds of mercury.
- Local economic development—Wind plants can provide a steady flow of income to landowners who lease their land for wind development, while increasing property tax revenues for local communities.
- Modular and scalable technology—Wind applications can take many forms, including large wind farms, distributed generation, and single end-use systems. Utilities can use wind resources strategically to help reduce load forecasting risks and stranded costs.
- Energy price stability— By further diversifying the energy mix, wind energy reduces dependence on conventional fuels that are subject to price and supply volatility.
- Reduced reliance on imported fuels—Wind energy expenditures are not used to obtain fuels from abroad, keeping funds closer to home, and lessening dependence on foreign governments that supply these fuels.

2 Wind turbines and wind parks

- A wind turbine is a mechanical assembly that converts the energy of wind into electricity. The three key elements of any wind turbine are the rotor, the nacelle—which contains the gearbox, the generator and control and monitoring equipment (see Figure 1)—and the

tower. Modern utility-scale wind turbines typically are equipped with three-bladed rotors ranging from 42 to 80 meters (138 to 262 feet) in diameter, contain generators with rated capacity of between 600 kW and 2 MW, and are mounted on towers that are between 40

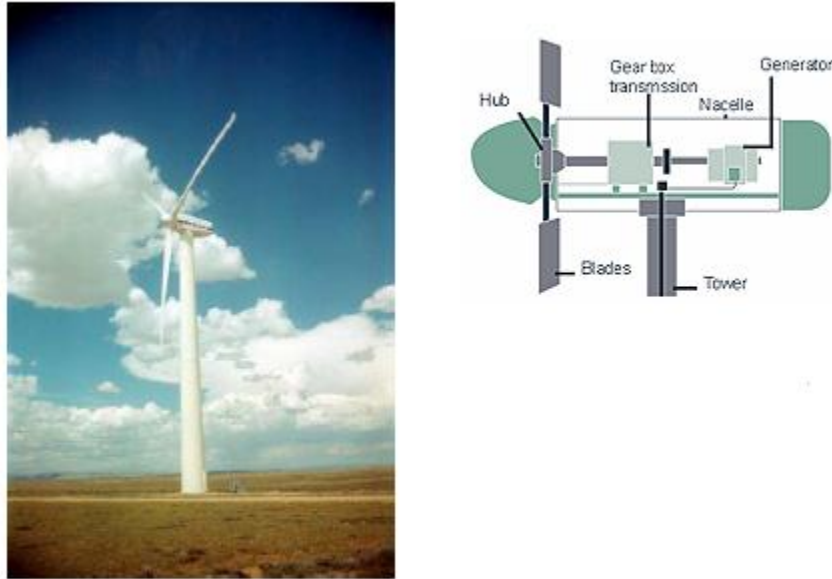


Figure 1: A 600 KW Vestas American Wind Technology.

and 100 meters (131 and 328 feet) tall (see Figure 1). A utility-scale wind installation, called a wind farm or wind park, consists of a collection of these turbines.

3 Tower Height

Tower height affects the amount of power that can be extracted by a given wind turbine, as well as the stresses on the rotor and nacelle. One kilometer above the ground, wind speeds are not influenced by the terrain below. The wind moves more slowly at lower heights, with the greatest reduction in wind speed found very close to the ground. This phenomenon, known as wind shear, is the key factor when deciding on tower height, as higher rotors are exposed to faster winds. In addition, the difference in wind speeds between the top and bottom of the rotor decreases with height, causing less wear on the turbine.

4 History of offshore wind

The first offshore wind park, a five MW installation near Vindeby, Denmark, came online in 1991. By the end of 2002, there were ten offshore wind farms in operation worldwide—all in Northern Europe—with a combined generating capacity of 250 MW. This represents a compound annual growth rate of 43%.¹⁹ This development has been fueled largely by the presence of good wind resources in the North and Baltic Seas and by the availability of everlarger, more efficient turbines with which to tap this resource. “Mega” turbines, those that can generate 1 MW of power or greater, reached large-scale production in 1998, and today “multi-megawatt” turbines with capacities of 2.5 MW are being installed in some locations.

5 Offshore wind resources

Average wind speeds over water are typically 20% higher than nearby locations on land. Thus, due to the cubic relationship between velocity and power, an offshore turbine can expect to capture 50% more wind energy than a similar onshore turbine. In addition, because of the lower wind shear at a given height above water compared to that same height above land, offshore turbines can be built with shorter towers and can last longer (see discussion of wind shear above).

Several foundation types are currently in use (see Figure 2). The mono pile foundation—used in more than half of existing offshore wind farms—consists of a single steel pile driven or drilled into the seabed. The gravitation foundation consists of a steel box sitting on the seabed that supports a cylindrical tube. The tripod foundation consists of three smaller piles connected by a frame to a central pile. Regardless of foundation type, the wind turbine’s platform and tower sit atop the foundation, above the water.

Due to technical and economic limitations, offshore wind farms are currently limited to relatively shallow waters. In the future, wind turbines could be mounted on floating platforms, tethered to the sea floor. These turbines could be situated in deeper waters where they would be invisible from land and could take advantage of even stronger open-ocean winds. Instead of feeding electricity into the grid, they could be used to produce hydrogen that would then be shipped or piped to shore. Preliminary feasibility studies suggest that facilities of this type could be built; however, further research is needed before such a wind farm can become a reality.

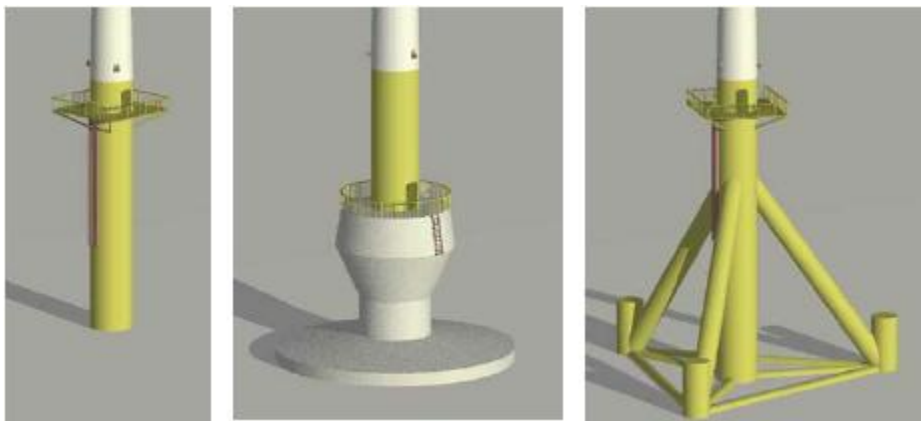


Figure 2: Foundation Types for Offshore Wind: Monopile, Gravitation and Tripod

6 Environmental benefits

The environmental benefits of wind power are felt locally, regionally and globally. Wind power can displace power from fossil fuel-powered plants, and thereby help to improve local air quality, mitigate regional effects such as acid rain, and reduce greenhouse gas emissions. On average, each MWh of electricity generated in the U.S. results in the emission of 1,341 pounds of carbon dioxide (CO₂), 7.5 pounds of sulfur dioxide (SO₂) and 3.55 pounds of nitrogen oxides (NO_x). Thus the 10 million MWh of electricity generated annually by U.S. wind farms represents about 6.7 million tons in avoided CO₂ emissions, 37,500 tons of SO₂ and 17,750 tons of NO_x. This avoided CO₂ equals over 1.8 million tons of carbon, enough to fill 180 trains, each 100 cars long, with each car holding 100 tons of carbon every year. Note that these figures are national averages and do not account for regional differences in fuel mix. Wind has the potential to displace relatively more emissions in areas where more heavily polluting fuels predominate.

7 Economics

While wind is a free resource, the systems used to capture the energy in the wind and convert it into electricity are not. Wind power production requires large capital outlays up-front, but does not incur fuel costs over the life of the plant. Wind producers also incur significant costs due to transmission infrastructure and regulatory frameworks that have been developed to suit the special characteristics of the fuels from which electricity has traditionally been produced—such as coal, nuclear and hydropower—but not wind. The many benefits of wind power accrue to producers, utilities and society. Benefits to utilities are discussed later in this section; benefits to society are discussed in the Environmental Impacts section below. Governments can help to spur wind development by revising regulations and providing financial incentives to wind power producers.

8 Cost measures

The installed capital cost of a wind farm includes planning, equipment purchase and construction of the facilities. This cost, typically measured in \$/kW, has decreased from more than \$2,500/kW in the early 1980's to less than \$1,000/kW for wind farms in the U.S. This decrease is due primarily to improvements in wind turbine technology, but also to the general increase in wind farm sizes. Larger wind farms benefit from economies of scale in all phases of a wind project from planning to decommissioning, as fixed costs can be spread over a larger total generating capacity.

Capital costs, which include the purchase of the turbine itself, construction of access roads and foundations, connecting to the grid and installation, account for about 70% of the total cost of energy. This is in contrast to fossil fuel-powered generation, which typically has lower up-front capital costs, but incurs fuel costs over the life of the system. Capital costs are now typically less than \$1000 per kW of generating capacity for large wind farms.

Maintenance costs account for about 20% of the total cost of energy. Much of this is for unscheduled, but statistically predictable, maintenance. These costs increase steadily with increased wear and tear on the turbines. Since the amount of wear and tear is roughly proportional to the amount of power produced, maintenance costs are roughly proportional to energy production. A reasonable rule of thumb for large wind farms is \$0.005/kWh.

Property taxes, land use, insurance, transmission/wheeling, substation maintenance, and general & administrative costs together account for the remaining 10% of the total cost of energy.

9 Economics of offshore wind

Two key factors differentiate offshore wind economics from those of onshore wind. The presence of stronger, less turbulent winds increases the revenue potential, while the location at sea increases construction and maintenance costs. These two factors tend to balance one another, resulting in a total cost of energy from offshore sites similar to that found at onshore sites.

Capital costs at offshore sites are between 30 and 70% greater than at onshore sites, according to a British Wind Energy Association report published in 2000. This is driven primarily by the high cost of building marine foundations, procuring installation equipment, and running submarine cables to carry the electricity to shore. However, these costs have decreased substantially in recent years, particularly because of improvements in foundation technology. Operation and maintenance costs are also considerably higher because ships are needed to bring personnel and equipment to the turbines and a turbine may be inaccessible when the seas are rough.

As mentioned, these additional costs are balanced by the increased energy production possible at sea. In addition, because of the reduced wind shear encountered over water, offshore wind farms are being designed to last for 50 years, rather than the more common 20-25 year lifespan found on land. With a major refurbishment after 25 years, the greater investment required for an offshore wind park can be amortized over roughly twice as many years as a similar onshore park.

High energy prices, proximity to major population centers, and the presence of excellent wind resources in the North and Baltic Seas have fueled the development of offshore wind farms in Northern Europe. In contrast, the first offshore wind farms in the U.S. are still in the planning stages. Lower energy prices and the availability of good wind resources inland have delayed the development of offshore wind there. However, more than half of U.S. residents live in coastal counties, so offshore wind farms in these areas could avoid the higher transmission costs faced by wind farms in remote locations. In addition, several states in the densely populated Northeast, including New Jersey, Connecticut and Massachusetts, have established Renewable Portfolio Standards (RPS), and wind may be one of the least-cost options available to meet these requirement

Chapter 1

Review Of Knowledge Development For The Design Of Offshore Wind Energy Technology

Offshore wind energy (OWE) is one of the emerging sustainable energy sources. Starting with the first offshore wind turbine in 1990, cumulative installed power has reached nearly 1500 MW in early 2009, mainly in the waters surrounding North-West Europe. Currently, government incentives are essential to the development of offshore wind farms, but in the long run, OWE will need to become competitive in the energy market under the same conditions as regular sources. Various activities, both academic and industrial, have contributed to the knowledge base that is needed to achieve the desired performance of offshore wind farms in terms of, for instance, cost, power quality, security of supply and environmental impact. This paper reviews the types of knowledge obtained with these activities, with the objective to identify points of attention for future research.

It is not the purpose of this paper to pinpoint specific areas for future research, which was done, for instance, by the European Technology Platform for Wind Energy. Rather, it reflects on the ability of academic research to contribute to design improvements for OWE and to stimulate thinking about a new direction. The next three sections review literature that contributes to the knowledge base that is needed to design for OWE. The first of these sections reviews object- and context-related knowledge, followed by a review of methodological knowledge. The last of these sections reviews the knowledge obtained from the experience of industrial implementation activities for OWE. After this literature review, the next three sections discuss characteristics of the design problem for OWE and of the academic research in order to identify where the two do not properly match.

The subject of the first of these sections is the appropriate perspective of academic research in terms of the system level and the level of detail. After this, some characteristics that are relevant for the usefulness of research results for industrial parties are discussed. The last of these three sections discusses the system design process from the perspective of a researcher. Based on the review and the discussions, the last section of this paper makes several suggestions about new directions for academic research to support technology development for OWE.

The emphasis of this paper is on the characteristics of the knowledge that is created rather than on the content of the knowledge. It is beyond the scope of this paper to discuss the validity and applicability of all knowledge relevant to offshore wind farm design. Therefore, most references in this paper only exemplify the statements and are not intended to be comprehensive

1.1 Design methodological knowledge

This section starts with a review of knowledge about what will be called here ‘design with a narrow scope’. Design with a narrow scope typically relates to design of a component or of a procedure. In case several disciplines are separately addressed during the design of a component, such as can be the case for aerodynamics and the structural dynamics of a blade, it refers to the mono-disciplinary focus. Design with a narrow scope is complementary to design integration, which will be treated after that. Design integration refers here to any approach that addresses several disciplines, several phases in the life cycle of a wind farm or several levels of scale.

1.2 Design with a narrow scope

To review knowledge about methodologies applied in design with a narrow scope, literature has been analysed that treats design of airfoils, blade, rotor, hub, shaft, main frame, gearbox, generator, control, yaw system, tower, foundation, farm layout, electrical power collection, electrical power integration, condition monitoring, installation procedures and maintenance strategies. Design methodologies are often not explicitly described in literature, but nevertheless, some observations can be made.

It is noted that the basis for these observations is predominantly design research in academia rather than design in practice. Much of the observations are based on research that does not aim specifically at offshore wind farms, but at wind energy in general. This research is considered relevant due to the overlap between the knowledge bases for onshore wind energy and OWE.

The predominant method encountered in concept selection is that of qualitative reasoning to compare the advantages and drawbacks of different options. Qualitative reasoning is particularly observed in literature that describes a specific design solution and its properties, although other quantitative methods may have played an unreported role. Qualitative reasoning has been observed in literature about, for instance, generator design, control design, support structure design and the development of installation procedures and access systems.

Many studies that address conceptual or preliminary design aspects appear to apply manual design iterations in which the knowledge and experience of the designer steers the process. However, this process is often not described explicitly and only one example is found of a diagram of such manual design process, in this case for suction buckets.

Case studies with a focus on providing contextualized knowledge usually do not go into details of the design process. Such case studies can be found for almost all aspects of design with a narrow scope and just a few examples are studies of airfoils, a composite hub and shaft, foundations and floating structures. Case studies are applied to obtain information about one particular case, to compare two or a few cases, or to perform a parameter variation study to assess sensitivities and explore the optimum. Parameter variation studies are presented, for

instance, for blades, for support structures, for in-farm power collection, for power integration and for maintenance strategies. The influence of uncertainties, model selection, constraints and other aspects are assessed more often and more explicitly for offshore support structures than for other elements.

Manual iterations for designs that encompass less understood physical phenomena sometimes use experimentation in the design loop, and this is particularly observed for boundary layer control devices, blades and scour protection. Evidently, experiments are also observed for other technology developments, but often not as a step in design iterations.

Under special circumstances, an analytical expression can be found for the design variables as a function of prescribed desired behaviour. Analytical methods are found for the preliminary design of airfoils, where inverse methods can be used to calculate airfoil geometry from a prescribed velocity or pressure distribution and for preliminary rotor design, where chord and twist distribution can be determined as a function of the desired induction factor and tip speed ratio. The resulting design is used as a starting point for further optimization and adaptation to meet all constraints.

There is literature about numerical optimization for almost all hardware components. Most commonly treated is parametric optimization, such as for airfoils, aerodynamic blade design, structural blade design and generators. Topology optimization is explored, for instance, for hub, shaft and mainframe, towers and wind farm layout. In these studies, the optimization methodology itself is usually an essential subject of research, in which case its feasibility or effectiveness is tested.

1.3 Integration of disciplines

Several components and services developed for OWE have design drivers that are based on various disciplines. For instance, soil mechanics, structural mechanics and dynamics, hydrodynamics and aerodynamics all play an important role in foundation design, and the generator is designed for both its electromagnetic and structural performance.

The development of integration of different disciplines in the design process is exemplified for blade design. Traditional blade design defines the external blade shape and aerodynamic properties first, after which the structural interior is designed. This traditional approach is reversed, where the design procedure starts with structural design, setting constraints for the aerodynamic design. A system design approach is applied; optimizing aerodynamics, structure and manufacturing simultaneously, but particularly the latter two processes still use extensive communication and manual design iterations. Simple models are developed to capture the main considerations and basic concepts of the aerodynamic and structural designs to yield analytical expressions for a preliminary design of a rotor. Several tools use an optimization algorithm for the aerodynamic and structural rotor specification, minimizing cost of energy. These tools include engineering models for the aerodynamics and mechanics of the rotor and parametric cost functions for the other components of the wind turbine. Most papers about generator design address only the active material of the generator, but McDonald et al presents an approach in

which the designs of the active elements of the generator and the structural elements are integrated.

The previous examples indicate that the development of analysis tools that integrate different disciplines is an important contribution to integrated design. Such tools have been made for various aspects of OWE. The tradition of making dedicated dynamic analysis tools for the aero elasticity of wind turbines has been extended for OWE by the addition of hydrodynamic loading models in programmes .

Also, the addition of integrated analysis of non-linear offshore foundation models has been researched. Wind turbine models have been added as scripts to general-purpose structural analysis tools, such as SAMCEF for Wind Turbines, enabling further possibilities for multi-physics analysis, numerical optimization and integration of different levels of detail.

The last possibility is particularly explored for blade design and gearbox design. For the analysis of the integration of large wind farms in the power system, many research projects have developed aggregated models of wind turbines for application in power system analysis tools. Tools have been developed to assess maintenance costs and availability of offshore wind farms, integrating information about wind and wave conditions, accessibility, logistics, reliability and repair procedures. It is noted, however, that these tools mainly model the logistics and obtain information about the other disciplines as pre-processed input data.

As observed earlier in this section, numerical optimization has been researched for the design of most components, and in cases where numerical optimization is added to an integrated analysis tool, this contributes to further integration of disciplines in the iterative design cycle. Numerical optimization with analysis tools that are specifically integrating disciplines for wind energy applications has at least been observed for the design of towers.

1.4 The appropriate perspective

Because OWE deployment distinguishes itself from its parental industries, i.e. onshore wind and offshore oil and gas, there are high expectations of opportunities for offshore wind farms to perform better when significantly large technology changes are implemented.

The previous sections described earlier knowledge development that contributes to finding these improvements. However, despite these research efforts and despite technological achievements in which the partakers can take pride, there is no evidence yet of a technological breakthrough of the extent of some of the bolder expectations.

This section and the next two analyse why the increase of the knowledge base for OWE technology has not yet led to such breakthrough. The analysis focuses on the abilities of the research to provide answers to engineering questions rather than the social and institutional conditions that are needed to support technological innovation. It is emphasized here that the deficiencies in previous research are analysed in terms of their ability to generate a technological breakthrough in OWE deployment, which is not necessarily the original intention of the research.

Chapter 2

Hybrid Configuration of Darrieus and Savonius Rotors for Stand-Alone Wind Turbine-Generator Systems

2.1 Introduction

The suitable hybrid configuration of Darrieus lift-type and Savonius drag-type rotors for stand-alone wind turbine-generator systems are discussed using our dynamic simulation model. Two types of hybrid configurations are taken up. Type A installs the Savonius rotor inside the Darrieus rotor and Type B installs the Savonius rotor outside the Darrieus rotor. The computed results of the output characteristics and the dynamic behaviour of the system operated at the maximum power coefficient points show that Type A, which has fine operating behaviour to wind speed changes and can be compactly designed because of a shorter rotational axis, is an effective way for stand-alone small-scale systems. Darrieus lift-type turbines, which are classified as vertical axis wind turbines, are advantageous because the mechanism of their power generation is not affected by the wind direction, and they can be set generators, gear boxes and controllers in low positions.

However, because of weak self-start-up characteristics, their start-up characteristics must be compensated through methods that provide a start-up device or that use a Savonius drag-type turbine in combination with them. The Darrieus and Savonius rotors can be combined by installing the Savonius rotor inside the rotational closed space of the Darrieus rotor (Type A) or by installing the former outside the rotational closed space of the latter (Type B). In this paper, the authors compare these two configurations focusing on not only the output characteristics of the hybrid turbines but also the net power extraction under field wind conditions while paying attention to instabilities in the start-up characteristics and when wind speed increases as dynamic characteristics of the system. As a result, the authors describe a rotor configuration that is useful for a hybrid turbine for a stand-alone power source.

2.2 The Darrieus Savonius hybrid turbine

The hybrid turbine has the Darrieus rotor on the main device, and the Savonius rotor combined permanently to the same axis as a start-up device. In order to obtain good start-up characteristics regardless of the wind direction, the Savonius rotor is divided into two (upper and lower), with the two parts having an attachment angle separated by 90° . In Type A, the Savonius rotor is installed inside the rotational closed space of the Darrieus rotor, emphasizing its compactness as a stand-alone power system. On the other hand, in Type B, the two rotors are connected outside

the rotational closed space in order to avoid air flow interference between the two rotors and giving priority to greater output from the wind turbine.

Because the values for the radius ratio of the Derries and Savona's rotors have a significant impact on the output characteristics of the hybrid turbine, this matter must be given serious consideration when designing a hybrid turbine. The calculated and measured results for a wind tunnel test device for the relationship between the rotor radius ratio RS/RD and the maximum power coefficient ratio CP_{max_H}/CP_{max_D} for the hybrid turbine and the Derries turbine alone. Here, the height of the Savona's turbine is fixed ($hS = 1.2$ m). For Type A, as the rotor radius ratio rises, the wake area for the Savona's rotor increases and the maximum power coefficient ratio falls. In addition, at $RS/RD > 0.3$, the maximum power coefficient ratio falls sharply because the Savona's rotor drives in reverse at the maximum power coefficient point for the Derries rotor.

On the other hand, in Type B, because the tip speed ratio for which the power coefficient for both rotors is at a maximum at $RS/RD = 0.3$ is equal (calculated using the rotational radius of the Derries rotor for the Savona's rotor as well), the maximum power coefficient ratio is also at a maximum. When $RS/RD > 0.38$, the maximum power coefficient ratio falls considerably due to the effects of the Savona's rotor driving in reverse. The relationship between the rotor radius ratio and the starting wind speed (calculated value) for the hybrid turbine. It is clear that by increasing the rotor radius ratio, the torque generated by the Savona's rotor rises, and the starting wind speed is lowered.

2.3 A wind turbine-generator system for a stand-alone power source

2.3.1 Outline of a stand-alone wind turbine-generator system

The wind turbine-generator system for a stand-alone power source being considered in this research consists of a hybrid turbine, the generator and storage battery as a load, and the controller. The storage battery supports smooth, reliable function for wind energy provided intermittently, and is essential as a stand-alone power source separate from the power system. In addition, the generator has an order to improve charging efficiency, by maintaining the output voltage matching the storage battery voltage.

2.3.2 Control method for system operation

In the authors' system, priority is given to extracting more wind energy, and so an operational method for variable speed control is used primarily for constant tip speed ratio operation so that the tip speed ratio is maintained with the power coefficient at a maximum regardless of variations in wind speed. In addition, at higher wind speeds, the operating mode is switched from constant tip speed ratio operation to constant speed operation. Thus, the system operating range can be extended by controlling the increase in the rotational speed. The desired operating points (relationship between torque–rotational speed–tip speed ratio– power coefficient) for the system when using the two hybrid rotor configurations ($RD = 1.0$ m). During operational control, dynamic equilibrium for input/output power must be established by controlling the turbine load

based on the variations in wind energy (wind speed), the input. In the authors' system, this is achieved by manipulating the output current of the generator. As can be seen in, the load control system is comprised of a main unit for feedback control of the rotational speed, whose desired value is the maximum power coefficient point calculated based on the wind speed, and the feed forward compensator which creates dynamic equilibrium for input/output power by controlling the load level at the desired operating point.

2.3.3 Evaluation of the dynamic behaviour of the system

The authors calculated and compared the dynamic behaviour of the systems using the two types of hybrid turbines employing a computational model for dynamic characteristics. Here, the operating behaviour is explored while bearing in mind the starting characteristics and the instability when wind speed rises.

2.3.4 Starting characteristics

The starting torque for the hybrid turbine is handled by the Savona's rotor in both hybrid configurations, and the starting wind speed depends on the static axial friction. Therefore, in Type B, it is clear that the axis friction torque rises as the axis weight rises, and the starting wind speed is higher compared to Type A. Next, in order to clarify the differences in the hybrid configurations as seen in the behaviour from start-up with no load to load control, the behaviour of the rotational speed at instantaneous release for the system ($RD = 1.0$ m) when the inflow wind speed is steady at 10 m/S . In both systems, load control starts when the rotational speed reaches 240 rpm. The authors were able to confirm that compared to Type A , Type B requires more time until starting load control after instantaneous release because the axial friction torque and the moment of inertia for the rotor are greater.

2.3.5 Behaviour under load control

First, the operational behaviour of Type A makes it clear that in a small-scale system ($RD = 1.0$ m) a circular path including the desired operating points shown by the dashed line is found. This is a result of the load controller (feedback control) functioning well such that the rotational speed with a delay with respect to the wind speed variation reaches the desired value (maximum power coefficient point) quickly. In addition, in a larger scale system ($RD = 10$ m), the rotor responsiveness falls as the moment of inertia rises. Therefore, a larger circular path obtains as a result of increasing the manipulated load due to large deviations of rotational speed with respect to the changes in the wind speed.

CHAPTER 3

Design And Control

3.1 Introduction

In recent years, the rotor size of new wind turbine designs has been significantly increased in order to extract more power from wind. As the rotor size increases, the flexibility associated with the rotor structure also increases and so does the influence that it has on the electrical transient performance of the wind turbine. When the size of the rotor increases, the frequency of the torque oscillations reduces and these oscillations may interact with the low-frequency modes of the electrical system.

In fixed-speed induction generator (FSIG) wind turbines, the induction generator acts as an effective damper, which helps to reduce the magnitude of the torque oscillations. However, it has been reported that these oscillations are still significant and must be taken into account when analysing the dynamic performance of FSIG wind turbines in transient stability studies. In the case of variable speed doubly fed induction generator (DFIG) wind turbines, which operate at constant torque, the damping contribution of the generator is low because the torque no longer varies as a function of the rotor speed. Hence, active damping techniques have been incorporated in both mechanical and electrical systems of the DFIG wind turbine. Recently, a power system stabilizer (PSS) has been proposed to enable DFIG wind turbines to contribute positively to network damping.³ In this case, if any of the frequencies of vibration of the rotor structural dynamics lies within the bandwidth of operation of the PSS then resonance may arise, which will affect the performance of both the mechanical and electrical systems of the wind turbine.

3.2 Blade bending dynamics

Wind turbine torque oscillations are due to the tensional flexibilities of the shaft and also to the bending flexibility of the blades. The tensional vibrations of the shaft can be represented using simple harmonic equations as explained in previous works. However, the representation of the blade oscillations is not straightforward due to the non uniform distribution of mass, stiffness and twist angle of the blades. For simplicity, these physical properties are assumed uniform in Eggleston and Stoddard to analyse the properties of the most dominant vibration mode of the blades. Nevertheless, if a more accurate representation of the dynamic properties of the blades is required then finite element techniques are employed as in Gradin.

The bending modes of a blade are defined in two orthogonal planes: (i) out-of-plane, which describes the motion of the blade perpendicular to the rotor plane, and (ii) in-plane, which describes the motion of the blade in the rotor plane. As the motion of the out-of-plane modes is normal to the direction of motion of the rotor, they do not directly couple to the drive train and therefore it is not necessary to include them in the model representation of the drive train dynamics. However, some of the in-plane modes directly couple to the drive train.

In the in-plane bending mode, there are two asymmetric modes and one symmetric mode of vibration. In the asymmetric modes, the three blades vibrate against each other, with no rotation of the rotor hub and thus there is no resultant torque applied to the shaft. In the symmetric mode, all the blades rotate in the same direction and the hub rotates in the opposite direction. The equation of motion of the rotor system can then be represented by a linear combination of these three rotor modes. However, only representation of the symmetric mode is important as it couples with the drive train. The asymmetric modes do not couple with the drive train and therefore may be neglected.

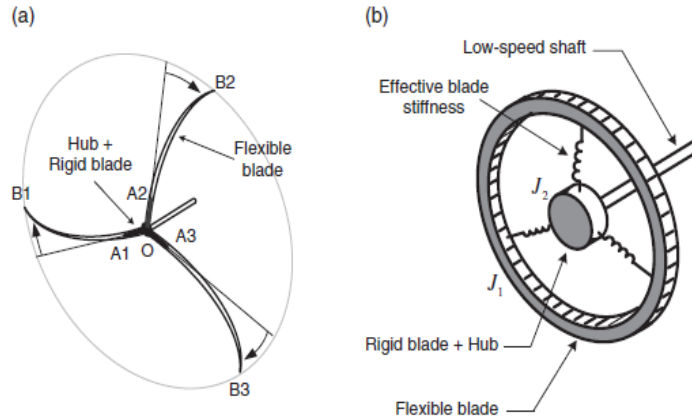


Figure 1. Equivalent blade inertia and stiffness of the in-plane rotor symmetric mode. (a) In-plane rotor symmetric bending mode. (b) Equivalent torsional representation

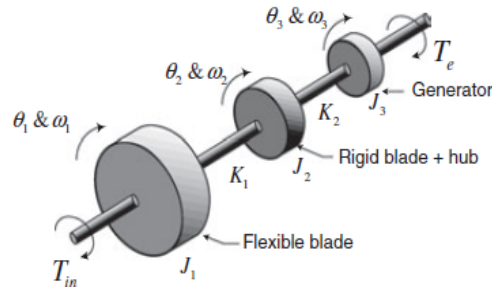


Figure 2. Three-mass model of drive train including blade and shaft flexibilities

3.3 Derivation of three-mass model

The rotor modes are defined in terms of mode frequency, mode damping coefficient and mode shapes. Mode frequencies and shapes are calculated based on the physical properties of the blade (mass, stiffness, twist angle distributions). The blade (which is tapered and twisted) is typically treated as a rotating cantilever beam, where the mass, stiffness and twist angle vary with the distance from the root. To determine the dynamic properties of the blade, finite element techniques may be used but this approach cannot easily be implemented in power system

analysis programs. Hence, to avoid the use of the finite element approach it is necessary to simplify the rotor dynamics as much as possible.

One way to achieve this is illustrated in (figure 1), where the blade bending dynamics illustrated in (figure 1) a is represented as a simple tensional system as shown in (figure 1 b) since the blade bending occurs at a significant distance from the joint between the blade and the hub, the blade can be split into two parts, OA and AB. The blade sections OA1, OA2 and OA3 are collected into the hub and have the inertia $J2$, and the rest of the blade sections A1B1, A2B2 and A3B3 are collected as a ring flywheel with inertia $J1$ about the shaft. The inertias $J1$ and $J2$ are connected via three springs, which represent the effective flexibility of individual blades.

By simplifying the rotor mode to two inertias connected via springs (figure 1 b) the drive train of the turbine can be represented by a three-mass model (figure 2) . $J1$ represents the inertia of the effective flexible blade section, $J2$ represents the combined inertia of the hub and the rigid blade section, $J3$ is the generator inertia, $K1$ is the effective blade stiffness and $K2$ represents the shaft stiffness (resultant stiffness of both the low-speed and high-speed shafts). The generator inertia $J3$, the shaft stiffness $K2$ and the rotor total inertia $J1 + J2$ are known variables. Therefore, two more equations are necessary to determine all five parameters of this three-mass model. The vibrating mode properties of the two- and three-mass models. The two vibrating frequencies in equation $f1$ and $f2$, can be obtained by conducting a spectral analysis of the low-speed shaft torque (through simulations). They can also be obtained using Campbell diagram analysis in Bladed, which directly provides these frequency components. Another possible way of determining these frequencies is by means of physical measurements (manufacturers are generally able to give these frequency values). In this work, these frequencies were calculated by conducting a spectral analysis of the low-speed shaft torque in Bladed.

The dynamic performance of FSIG and DFIG wind turbines during a fault was assessed for various representations of the rotor structural dynamics. It was identified that modelling the shaft flexibility only may not provide a true representation of the rotor dynamics. A three-mass model that takes into account both shaft and blade flexibilities was then derived. However, representation of both shaft and blade flexibilities increases the order of model, which may not be desirable for large power system studies.

Therefore, the three-mass model was reduced to an effective two-mass model, which takes into account both shaft and blades flexibilities but that only represents the dominant, low frequency component of the rotor structure. The fault studies conducted with FSIG and DFIG wind turbines illustrated that the torque oscillations of a two-mass model with only shaft flexibilities were more benign than that obtained with the effective two-mass model. The two-mass model with representation of only shaft flexibilities may therefore not be appropriate for transient stability studies as some torque oscillations, which may interact with the electrical system, are not fully taken into account. If the two mass model parameters are determined based on experimentation, it should correspond to the effective two mass model parameters.

3.4 Variable speed variable pitch wind turbine control objectives:

Variable speed variable pitch wind turbine operation can be separated into three major operating regions:

- Region 1: Below cut-in wind speed (V_c)
- Region 2: Between cut-in wind speed and rated wind speed (V_r)
- Region 3: Between rated wind speed and cut-out wind speed (V_{co}).

In Region 1:

The wind speed is too low for the wind turbine to be operating.

Region 2:

The turbine operates in variable speed mode to capture as much energy as possible.

In Region 3:

Excess power in the wind is shed by maintaining the turbines rated rotor speed most commonly through blade pitch control and generator torque control.

In addition to these speed/power control measures, by adjusting the blade pitch and generator torque, it has been shown that fatigue loads in the drive-train, blades and tower can be reduced by multivariable controllers.

3.5 Non-linear control methods

The predominant methods of controlling loads and power have been linear control methods utilizing the blade pitch and generator torque actuators. Common controller types are model-based Linear Quadratic Gaussian (LQG) control and Proportional Integral Derivative (PID) control.

The wind turbine, however, is highly non-linear with respect to its aerodynamics. As the wind speed, rotor speed and or blade pitch changes, the power capture changes nonlinearly according to equation (1).

$$P_r = \frac{1}{2} \rho V^3 C_p (\lambda, \theta) \quad (1)$$

Where ρ is the air density, ωr is the rotor speed,

θ is the blade pitch

R is the radius of the rotor, V is the effective wind speed

C_p is the power coefficient.

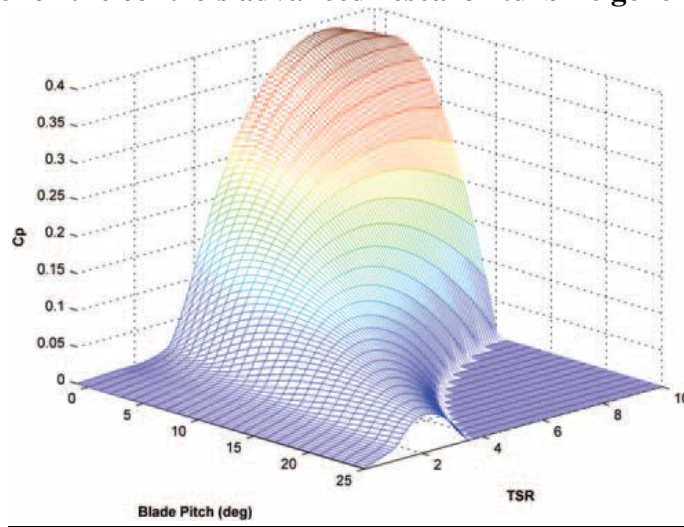
The tip speed ratio λ is described in equation (2).

$$\lambda = \frac{\omega r}{V} \quad (2)$$

Because the wind field varies spatially over the rotor swept area, we designate V as the effective wind speed, the wind speed at which the current rotor power would be extracted given the rotor speed and blade pitch.

A quasi steady-state representation of the C_p curve (Figure 1) is shown for the Controls Advanced Research Turbine (CART) at the National Renewable Energy Laboratory, USA, generated using WT-PERF, (program to predict wind turbine performance) which can produce power coefficient plots for wind turbines given aerodynamic data.⁴ This plot shows that equation (1) is highly non-linear. Because of the nonlinearities, controllers designed using linearized models are only optimal near their designed operating point.

Figure 1. C_p curve for the controls advanced research turbine generated by WT-PERF



The work concluded that the most appropriate controller for further investigation was the Feedback Linearization controller due to its relatively high control performance and low actuator usage.

3.6 Modelling and control Design

Three controllers are described in this section. A single input single-output (SISO) GSPI is used as a baseline for which to tune the remaining controllers. This controller is chosen as a baseline as it is prevalent in literature and also has standard design guidelines. While this controller has the ability to reduce the effects of aerodynamic nonlinearities, it is a SISO controller that manipulates the collective blade pitch in order to control rotor speed.

An linear quadratic controller (LQR), also common in the literature, is used to show the improvement in drive-train load control by using a multi-input multi-output (MIMO) controller with both collective pitch and generator torque actuators. While this controller can have added control objectives when compared with the GSPI controller, it does not include the effects of aerodynamic non-linearities.

The final controller (FL) to be described is an FL controller based on work by Thomsen.¹⁶ This controller is both MIMO akin to the LQR and can reduce the effects of aerodynamic non-linearities similar to the GSPI controller.

This controller, however, requires an estimate of the wind speed to function. Because the wind speed varies spatially of the swept rotor area, it is difficult to obtain an accurate value of the effective wind speed providing torque to the rotor.

All controllers have been designed using models based on the CART (Figure 2). The models use the properties of a 600 kW, two-bladed, variable speed variable pitch horizontal axis wind turbine at the National Wind Technology Centre in Colorado.

The turbine is well instrumented with turbine structural load data, generator power output data, generator speed data and rotor speed data, which help facilitate the implementation and testing of various control algorithms.

The turbine has a rated wind speed of 13 m s^{-1} and a cut-out wind speed of 26 m s^{-1} . The rated rotor speed for this turbine is 41.7 rpm. The CART pitch actuator has rate and acceleration limits of 18° s^{-1} and 150° s^{-2} , respectively, 21 and has an allowable RMS pitch acceleration of 90° s^{-2} .



Figure 2: The cart

3.6.1 Modelling

3.6.1.1 Non-linear model

In order to design controllers for the turbine system a turbine model is needed. For the FL controller, a non-linear five state control affine model (only non-linear with respect to the states and not the control input) of the system is used.

This can be represented by equation (3):

$$- \quad {}^2V_{\omega}^3 C_p(x, \lambda) \quad (3)$$

The turbine dynamics have now been defined as a function of the power coefficient (C_p), tip-speed ratio (λ), rotor power (P), rotor inertia (J_r), wind speed (V), drive-train damping (D_s), drive-train spring constant (K_s), gear ratio (N_g), actuator time constants (τ_{θ} , τ_T), drive-train inertias (J_g), states (x), and control inputs (u).

3.6.1.2 Linear model

For linear control design, a linear model of the wind turbine is necessary. Instead of explicitly linearizing the previous non-linear model, which has a simple aerodynamic representation, a four state linear model is obtained using FAST's linearization capabilities.

This model has two DOFs: generator rotation and drive-train torsion. The linear model obtained from FAST is in the form: $\dot{\mathbf{X}}_m = \mathbf{A}_m \mathbf{X}_m + \mathbf{B}_m \mathbf{u}_m + \mathbf{B}_{d,m} \mathbf{u}_{d,m}$ (4)

$$\dot{\mathbf{X}}_m = \begin{bmatrix} \dot{\phi} \\ \dot{\delta} \\ \dot{\omega}_r \\ \dot{\delta} \end{bmatrix}, \quad \mathbf{u}_m = \begin{bmatrix} T_g \\ \theta \end{bmatrix}, \quad \mathbf{u}_{d,m} = V$$

ϕ is the rotor azimuth position, ω_r is the rotor speed, δ is the drive-train torsion, θ is the blade pitch angle, T_g is the applied generator torque, and V is the effective wind speed.

3.7 Gain scheduled proportional integral controller

Proportional integral controllers are commonly used in wind turbines for rotor speed control. In addition, these controllers are often augmented with non-linear controller gains to reduce the effects of turbine non-linearities. A GSPI controller is used as a baseline controller against which the LQR and FL controllers are compared. Although, there are many architectures for applying GSPI control including those for MIMO system .

3.8 Linear quadratic regulator (LQR)

Using an LQR allows us to use multiple actuators to control multiple turbine states with a single controller. In this paper, generator torque and collective blade pitch are used to control rotor speed, generator power and drive-train loads.

To improve performance by avoiding steady state power errors we introduce to the previously derived linear model a state for the integral of the power error.

3.9 Control design

This is a linear system for which an LQR can be designed by assigning v as the new control input. The input v is still a two-element input vector, where the first element is no longer the blade pitch input. It has now been transformed into a non-linear function with little physical meaning except that it does affect the blade pitch. The second element remains the generator torque input.

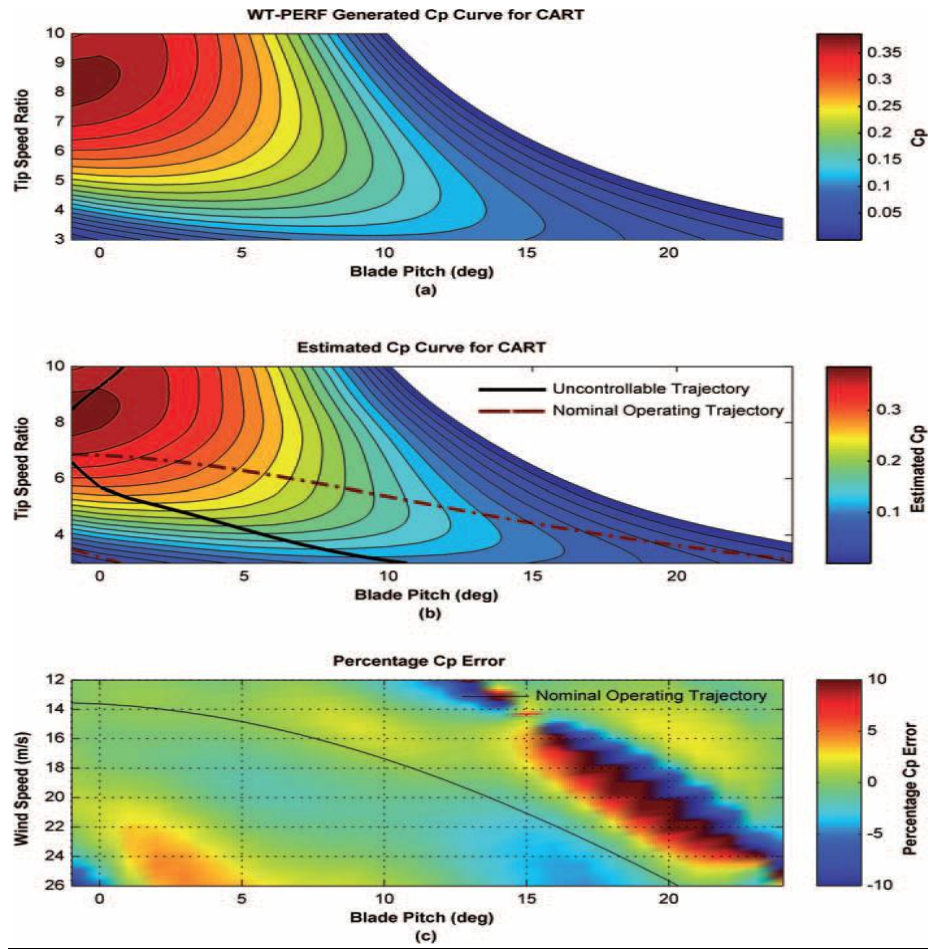
The transformation $T_{\zeta}(x)$ has been proven to be a diffeomorphism (invertible and differentiable transformation)

If $0.1 \lambda 10$ and $-1\theta 25$ by checking that is non-singular in this region. This allows the linearizing control law to be valid in this region, in contrast to direct linearization (used to produce linear controllers), which is only accurate at a particular operating point.

The linearizing control law equation requires the calculation of all its derivatives to be (Lie derivatives) to be possible hence an analytical expression for C_p needs to be obtained.

The figure also shows that:

1. Original C_p curve crated by WTPERF, the estimated C_p curve, and the percentage error between the polynomial and the actual C_p curves. It can be seen that along the nominal operating trajectory the error in C_p is within 5%.
2. A further condition that needs to be met is for $L_g L_f x_1$ to be non-singular. This follows the trajectory where power is not sensitive to changes in pitch angle (uncontrollable trajectory in Figure b).
3. Although this condition occurs independent of controller choice, which means any control signals in this region will be ineffective (being a property of the turbine), it is of critical importance with the FL controller because it affects the controllers' ability to produce bounded control inputs. This condition does not intersect with the nominal operating trajectory if the system is controlled well.



3.10 Conclusion

Speed control performance of the FL controller is superior to a LQR at low wind speeds; however, no performance enhancements are seen at higher wind speeds. Power control and drive-train load reduction performance are poorer than LQR at low wind speeds but better at high wind speeds.

In order to achieve these levels of performance, the controller pitch actuator acceleration exceeded the limits of 90° s^{-2} RMS. It is important to review whether the benefits of the controller outweigh the cost of the additional actuator usage. Speed control performance degradation at high wind speeds is determined to be due to the effects of un-modelled dynamics, errors in approximating the C_p curve for the wind turbine with a polynomial, and using a static C_p curve to model the turbines power function which is inherently inaccurate in a dynamic system. Future work should include analysis using robust FL techniques to help reduce the effects of model uncertainty.

CHAPTER 4

The System Design Process

4.1 Efficiency of the search for solutions

The enormous number of alternative technical concepts for OWE calls for a process that is highly effective in terms of the time needed to find better solutions. Previous academic and industrial research proves particularly strong in performing design studies of sub-systems, such as support structures. These design studies provide knowledge about the design solutions as well as about the methods used to analyse their behaviour and value.

However, these studies generally do not provide information about the effects of integration of such solutions in an OWE conversion system and about possible system trade-offs. Because the value of the design solutions on the system level is left uncertain, much additional work is needed to determine whether the results of these studies can positively affect the development of OWE.

Only very few research projects provide design solutions for all main parts and procedures of an offshore wind farm. The foremost results of these studies are information about the design of the individual parts and the technical and economic feasibility of the entire system. The scope of these studies is much broader than in typical industrial design, covering the entire wind farm and at the same time dealing with conceptual variations of details that are normally fixed or at least restricted (e.g. pitch or stall control). However, this scope is also the Achilles heel of this approach, as the number of labour-intensive conceptual design variations that can be covered in the project is far less than the number of possibilities. The necessary pre-selection of concepts is based on qualitative information and expert judgements, but because the concepts of interest are relatively extraordinary, the available knowledge is limited.

A solution-driven approach is thus complicated by the incompatibility of the desire to think out of the box and the need to make quick judgements for many design options. Several recent industrial developments bypass this dilemma by choosing a particular conceptual configuration in a very early phase, which is then developed to more detail and eventually even a prototype. For the aero generator, a V-shaped vertical axis rotor is selected; Darwind selected the direct drive concept Blue H Technologies has taken a two-bladed rotor with a very high tip speed as a starting point; and the yet unpublished concept selected by 2-B Energy also allegedly deviates in several aspects from regular concepts. This approach may lead to the desired breakthrough, but it is evidently risky, costly and not very efficient in exploring the design options.

A drawback of providing design solutions by case studies is the limited potential for reuse of the judgement of the design results, since the designs are made for particular conditions. Given the uncertainty of effects of changes in the conditions, only obvious advantages will be convincing. Some research supports design efforts by providing better design methods.

An inherent advantage of methods is that they are suitable for reuse and can more easily be transferred from academia to industry. As observed in the review, the literature in this area is dominated by studies of optimization methods. In most cases, these studies address only optimization of the dimensions of a selected concept, but a few studies aim at topological optimization, for towers, or even the optimum architecture as done for horizontal axis rotor-nacelle assemblies.

Although systems engineering is a methodology presumably suitable for offshore wind farm design, experience with this methodology is hardly described. Moreover, apart from giving a broad outline of the design philosophy, most papers discussed in the review do not describe the methodology they apply. Many papers that do present design methods actually treat methods that are used in the analysis phase instead of methods that aid the synthesis process directly. For example, Salameh Z, Kazda L. 1986. Analysis of the steady state performance of the double output induction generator *IEEE*

Transaction on Energy Conversion 1(1):26-32. the term design in their title, but they actually address modelling of wind, wakes, waves, currents and structure-soil interaction, the selection of load cases, and the simulation of dynamics and resistance. All in all, there appears to be little research that aims at improving the efficiency of finding better design solutions by means of new methodologies.

Many research activities contribute to foundational knowledge, needed to perform simulation and analysis of provisional design solutions. Most of the design-related studies reviewed for this paper are solution oriented and contribute to object- and context-related knowledge, particularly by means of case studies. Studies that put more emphasis on methodologies largely target optimization methods.

It was identified that conceptual change of the main sub-systems, which might have significant effects on the design of other sub-systems, is a potential area for technology development for OWE. The appropriate system level to analyse the effects is the long-term international development of OWE. This development is based on many asynchronous design processes at various different companies, and several interactions between these design processes are formed by market mechanism rather than by design activities.

An enormous resource of designers and design knowledge is employed in industrial activities, and academic research would do well to tap into these resources. Industry is strongest in design with a narrow scope, focusing on the part that is supplied, but it is weaker in two other areas. First, it has less knowledge of design of alternative concepts, but there is a strong tradition in academic design research to complement this weakness.

Second, it has little support for the integration of their parts in long-term OWE developments. Previous activities brought integration into the picture by getting designers out of the companies into an integrated design project, but this failed to bring integration into the companies. New research could aim to stimulate technology developments inside companies by supporting design integration in their in-house processes. This would most effectively be done with methodologies and tools that can be transferred from academics to industry and that contain the knowledge

needed for integration. One of the points of attention would be the support of consistency of the various design processes and the compatibility of the design solutions.

The search for new design solutions is currently based to a large extent on qualitative reasoning, intuition, expectations and maybe even wishful thinking. Quantitative information is limited to selected solutions of case studies. The search process would benefit from the availability of quantitative information that can be generated quickly for different conditions. Contrary to trend analysis, this information should be based on technological principles, such that it can be used to assess the differences between different technologies and to identify the origin of benefits and drawbacks. Previous studies have resulted in engineering models that provide such information, but the applied principles could be further exploited and made suitable for integration support. Particular aims would be to sharpen expectations, to assess the potential of new ideas, to identify critical components and procedures, to identify critical requirements and environmental conditions, to support decisions, to quantify trade-offs, to support technical budgeting and to rank design interactions between different parts.

Quantitative information is only valuable when it is sufficiently accurate and when there is enough insight in the uncertainties. However, information about the accuracy of preliminary design results and about development risks of new technologies is rarely addressed in current research. There is a need for knowledge about these issues, both with respect to uncertainties associated with specific technologies and with respect to the uncertainties of the effects that that technology will have on other elements of the system.

the analysis of previous design research and the involved processes leads to a plea for a different direction for the support of development of OWE technology by academic research. Research of less common concepts by means of desktop design studies should remain and should be focused on confined areas. However, integration studies should move away from a solution-oriented design approach and should move towards methodologies to support design integration in the asynchronous design processes in the industry. Only then can the full capabilities of design in the industry be employed in this quest.

Wind energy is currently the fastest-growing source of electricity in the world. Wind power investment worldwide is expected to expand three-fold in the next decade, from about \$18 billion in 2006 to \$60 billion in 2016. In the U.S., where wind currently only provides about 1% of the nation's electricity, wind has the potential to provide up to 20% of the nation's electricity without major changes to the nation's electricity distribution system. However, there are still many unsolved challenges in expanding wind power.

We will overview the standard controls as well as recently developed advanced controls for variable-speed, horizontal axis wind turbines. For a more general tutorial on wind turbines and the references therein It is becoming more common for modern turbines to provide individual pitch actuators at each blade so that the number of control inputs available to the system designer is increased above the traditional generator torque control.

Pitch commands to individual actuators are depicted schematically. In addition, force/moment sensing or accelerometers can be installed at each blade individually as well as on the nacelle and tower. These additional inputs and outputs combine with the fact that the turbine structural modes couple with the drive train and pitch actuation through torque and bending moments to make the wind turbine an inherently multi-input-multi-output (MIMO) system.

Indeed, as turbine size increases and weight/cost considerations motivate accommodation of increased flexibility, it becomes more critical to take into account coupling between different structural modes and to utilize more sophisticated control methods to deal with these effects. Further, increased flexibility of turbine structures brings to the fore-front the task of mitigating damaging loads at the blade roots and the tower base. Advanced control methods for addressing these issues have been investigated for well over a decade, but apparently most commercial systems are still implemented using multiple single-input-single-output (SISO)

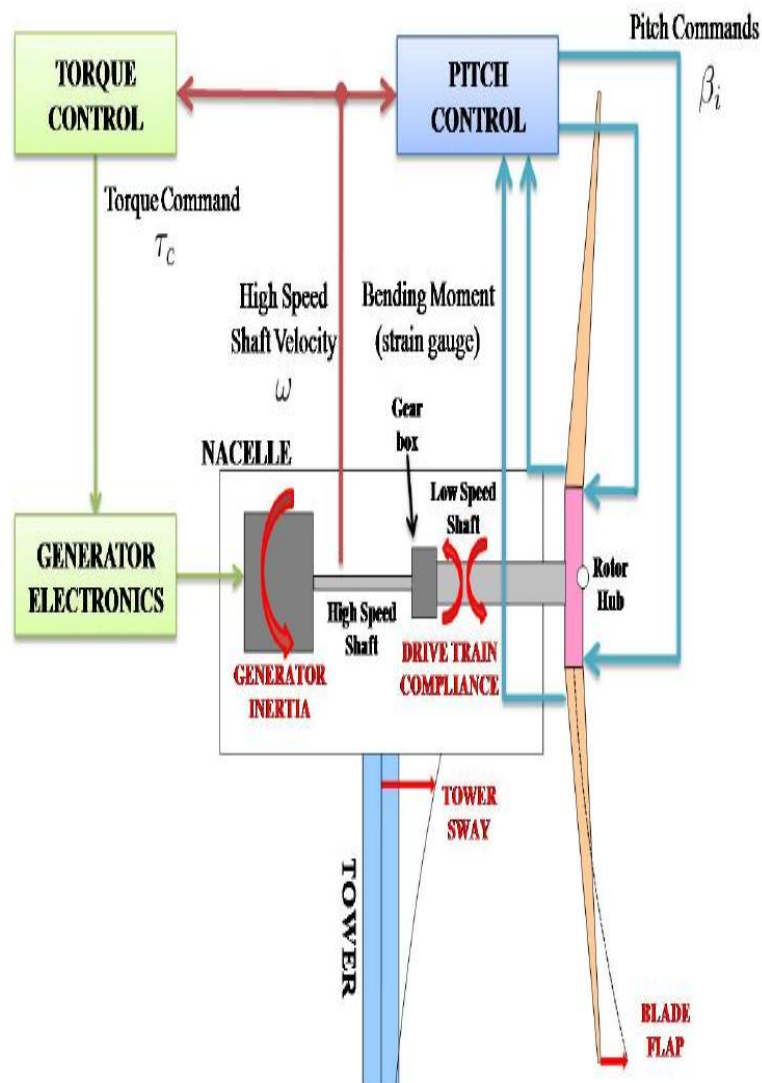


Fig. 1. Common turbine control loops. Generator speed is often the only measurement for both generator torque and pitch control. Supervisory control (not shown) can have additional measurements including local anemometer-based wind speed. More advanced turbines might also include individual blade bending moment/strain measurements and instrumentation for tower/nacelle accelerations.

loops which shows two different controllers for the generator and pitch control loops; if the pitch commands are identical and based only on the high speed shaft velocity, then this configuration comprises two SISO controllers operating independently of each other. In contrast, advanced control approaches are distinguished by the hallmarks that plant uncertainty is explicitly accounted for in the design, a multi-input, multi-output (MIMO) controller is designed that accommodates coupling between loops, or a robust MIMO method is utilized. Additionally, methods employing adaptive or nonlinear techniques have also been reported.

Our intention here is to provide an overview of linear controller objectives and designs utilizing deterministic approaches applied to blade pitch and torque control. In addition, we will demonstrate how any feedback architecture can be augmented with a disturbance feed forward compensator utilizing wind measurements that may be available from novel technologies on the horizon.

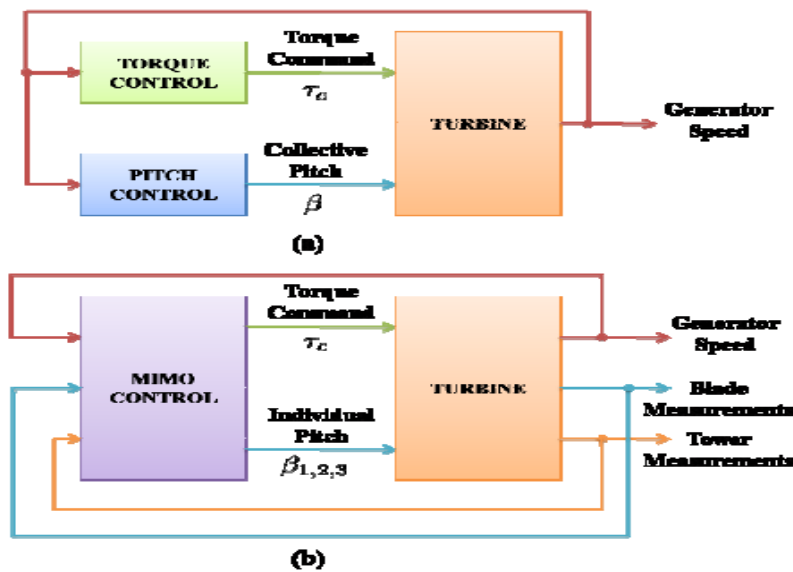


Fig. 2. (a) Traditional turbine control is based on generator speed feedback alone. Torque and pitch controllers are treated as separate SISO loops. (b) MIMO control is a hallmark of the controllers in ongoing research; the controller has access to individual blade measurements in addition to generator speed and may also utilize measurements of tower motion and strain.

4.2 Regions of operation and linear models

In this section we characterize a linearized model of the turbine structural dynamics and view the generator as simply a static (unity) gain that translates commanded torque instantaneously into mechanical torque.

A wind turbine is inherently nonlinear and time varying. Aerodynamic torques and bending moments depend nonlinearly on wind speed, pitch angle, and tower and blade deflections. Further, there is variation as the rotor turns to position the blades in a turbulent wind profile that

varies spatially with respect to the rotor disk even in constant wind conditions. Nevertheless, good results have been obtained using linear, time invariant models of the turbine.

Many of these models are developed analytically by linearizing a turbine model at a particular operating point using blade element momentum (BEM) theory to determine aerodynamic loads and the method of assumed modes to model turbine flexure.

FAST simulates the turbine in constant (and possibly non-uniform) wind conditions to find a solution that changes only as a function of rotor position and then computes a linearized model by calculating the coefficients describing the perturbation of the system configuration/state with respect to a set of specified input perturbations.

Linearization commonly renders a kinematic system of the Form (1) where the $M(q)$, $C(q)$, $K(q)$, $F(q)$, and $F_d(q)$ coefficients are dependent on the operating point and can be parameterized by the rotor azimuth position. The vector of configuration variables represents deviation of the turbine away from the nominal operating point (at each rotor position).

We evaluate a turbine model based on the 600kW, 3- bladed, upwind, variable-speed, horizontal-axis Controls Advanced Research Turbine (CART3) located at the National Renewable Energy Laboratory (NREL).

The CART3 has a rated rotor speed of 41.7 revolutions per minute (rpm); the velocity of the low-speed shaft (connected to the rotor) is stepped up by a gear box so that the high-speed shaft and generator run at a rated speed of 1800 rpm. Changes in the linearized turbine model occur with operating point (total wind speed, rotor speed, and blade pitch) as the turbine operates in different regions.

These regions can generally be described as follows:

In Region 1:

The wind speed is too low to warrant turbine start-up. The blades are pitched at full feather (the pitch angle that generates minimum aerodynamic torque). Once the wind speed is large enough (above 5 m/s for the CART3) for machine start-up, the blades are pitched to the normal Region 2 angle. At nominal pitch, the aerodynamic lift is in a direction to produce torque and accelerate the rotor. Once generator speed reaches 430 rpm for the CART3, generator torque is turned on and the turbine begins power production in Region 2

In Region 2:

- The wind speed and the generator torque are below “rated.” Blade pitch is held constant at the optimal value that gives maximum aerodynamic torque. Each wind speed has a corresponding rotor speed at which the greatest possible aerodynamic torque is generated. It turns out that when the blade pitch is held at the optimal, there is a constant value, or tip speed ratio (TSR), (where r is blade radius) that maximizes aerodynamic torque. Normally a function of TSR and pitch, the fraction of aerodynamic power obtained from the total wind power is a maximum when. So, the control objective in Region 2 is to command torque so that w tracks with and gives a TSR.

In Region 2½:

- The wind speeds are approaching those that provide rated power. This is a transition region where the torque command is commonly computed as an affine function of generator speed such that rated torque is reached before the rated generator speed.

In Region 3:

- The wind speed is at or above (11.7 m/s for the CART3) that which will generate rated power. The generator torque is held constant at rated, and blade-pitch control is used to limit aerodynamic power by regulating turbine speed at the rated speed. Advanced controls are also designed to mitigate loads on the blades and tower.

The frequency responses of perturbations in the generator high-speed shaft velocity (HSSV) and flap bending moment at the root of the blades are computed for pitch perturbations made collectively on all blades. This computation is done for the linearized model at each azimuth position.

Fig. 3 shows the envelope of magnitude responses obtained by finding the minimum and maximum gain at each frequency over all responses. The top plot depicts HSSV response and the bottom plot depicts bending moment response. Blue solid lines denote the envelope from models obtained in the presence of shear and green solid lines denote the envelope obtained from models in uniform conditions. A “mean” model representing the turbine over all azimuth angles is obtained by computing the average of each of the coefficient matrices in (2). In Fig. 3 the response of the mean models are denoted by dashed red and magenta lines for shear and uniform conditions, respectively

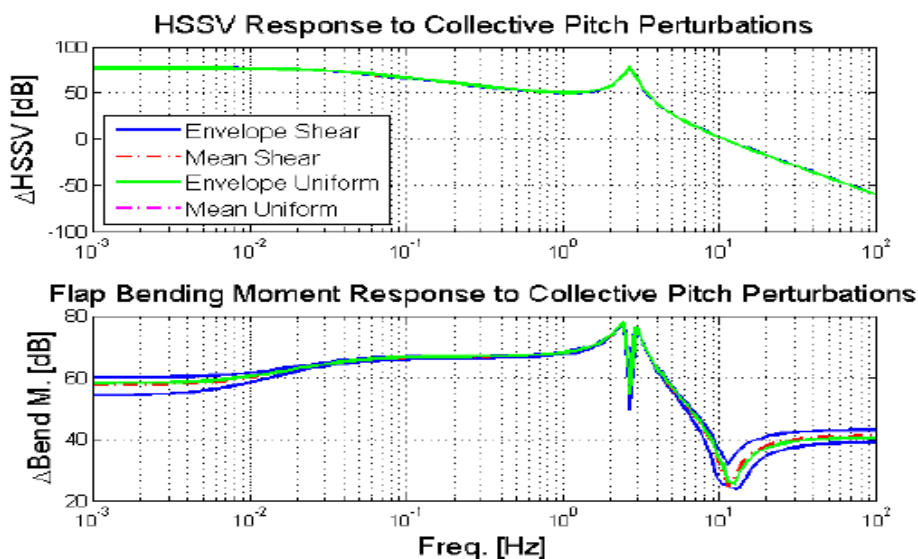


Figure 3: Shows the study of turbine linear model dependence on rotor azimuth position.

Fig.4. Perturbations in HSSV response for different operating regions and wind speeds. The lower two envelopes (solid blue) show the changes in response to torque and pitch perturbations across a range of Region 2 wind speeds (5–13m/s). The two upper envelopes (dashed red and green) show the change in response to pitch perturbation across various Region 3 operating points. There is a large variance in HSSV response to turbine pitch throughout Region 2 (5–13m/s). In Region 3, where pitch is adjusted to maintain a rotor speed of 41.7 rpm, HSSV response varies less, both with varying wind speed (green, 16– 24 m/s) and with pitch (red, 4–18 deg, wind speed = 18 m/s).

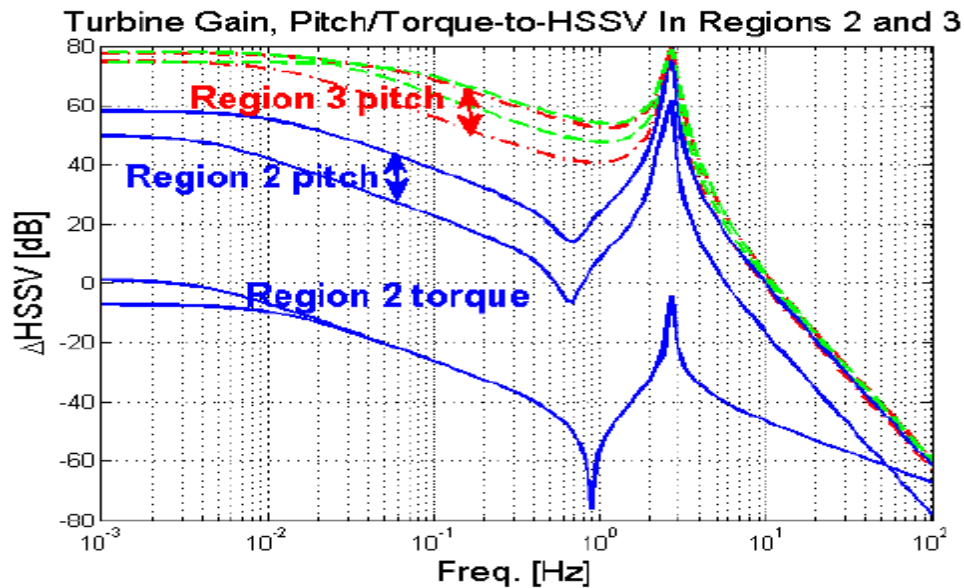


Figure 4, Perturbation in HSSV response for different operating regions and wind speeds.

Region 3 Control:

Referring to Fig. 1, generator speed is measured and passed to both the torque and pitch controllers. Classical proportional-integral-derivative (PID) control techniques are typically used to design the blade pitch controller for Region 3 [19] to regulate turbine speed in the presence of varying wind conditions where is the generator or rotor rotational speed error. Using only rotor speed error as feedback, the pitch command is necessarily collective (the same for all blades). The pK , IK , and DK gains are chosen to give “desired” closed-loop characteristics. Further discussions on methods for choosing these gains are found. Often, the standard PID control is augmented (multiplied) with notch transfer functions to add damping to known resonance.

New Control Strategies Enabled by Novel wind measurement techniques:

Currently, most control algorithms depend on measurements from turbine structure and drive train for use in the control feedback. Often these turbine measurements are unreliable or exhibit

delayed response to disturbances acting on the turbine. This constrains the controls to react to complex atmospheric disturbances after their effects have been “felt” by the turbine. Thus, there is an inherent lag between the time that a disturbance arrives and the time that the control actuator begins to mitigate resulting loads. A considerable advantage in load mitigating capability can be attained by measuring atmospheric phenomena upwind of the turbine before they impact the turbine rotor. The needed control actuation signals can then be prepared in advance and applied as the inflow to the turbine changes with potentially significant load mitigation improvement.

New lidar technologies are capable of measuring velocity upwind of the turbine with sample rates in the 10’s of Hz [37]. With these measurements, it is possible to design preview controllers as depicted in Fig. 8 that can adjust pitch (and/or torque) as necessary before wind disturbances arrive at the turbine.

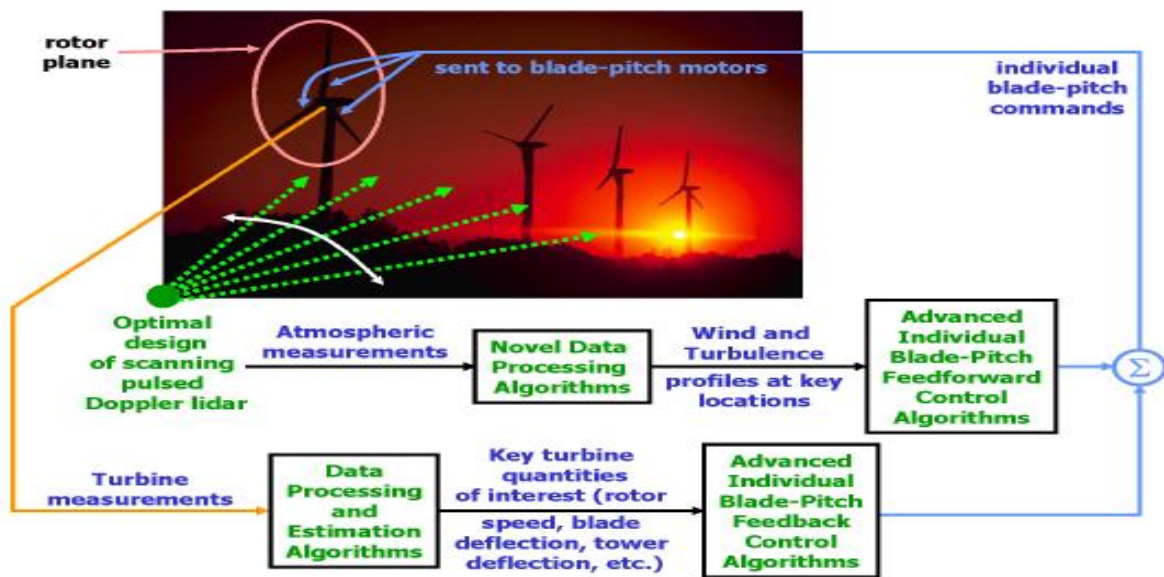


Fig. 8. Availability of lidar measurements enables the implementation of disturbance feedforward methods.

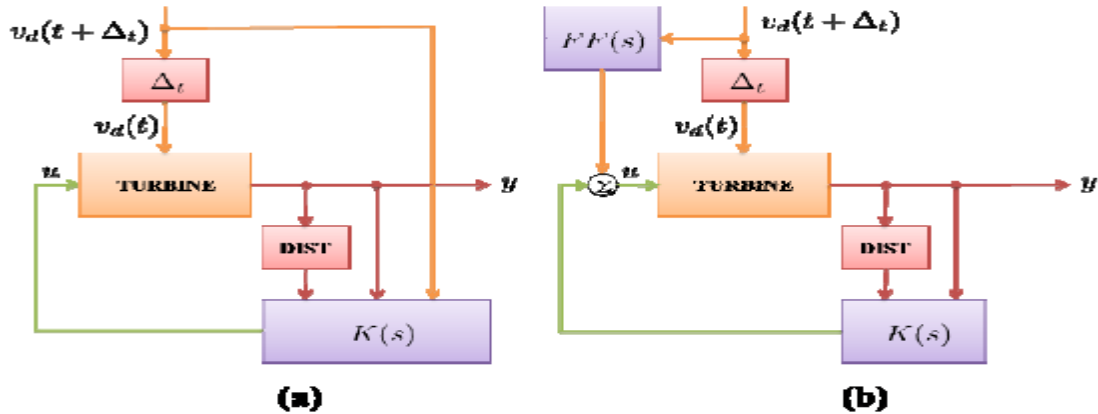


Fig. 9. Preview control uses “look-ahead” measurements of incoming wind disturbances to generate pre-actuation. (a) Compensation designed in conjunction with feedback control. (b) Stand-alone, feedforward control based on plant inversion.

The preview control can be designed in unison with the feedback control [36] as depicted in Fig. 9(a) or separately from feedback [38] as in Fig. 9(b).

Proper characterization of the wind inflow to a turbine is important for improved turbine design. Concentrated wind gusts, rapid wind direction changes, or passage of energetic atmospheric structures impose critical loads on individual wind turbines and blades. These extreme events decrease turbine lifetimes, cause component failures, and can even threaten catastrophic machine failure.

It is crucial to understand the complex wind inflow to the turbine in order to design load mitigating controls which adequately account for these complex atmospheric phenomena.

Preliminary investigation of preview, feed-forward techniques indicate the promise of tantalizingly large Improvements in controller performance. Implementation of such methods relies heavily on new measurement technologies that each come with their own, characteristic distortion and noise issues [39]. Even if these prove to be surmountable, there remains the fact that an upstream, wind, velocity profile will hardly be the same when it arrives at the turbine. Modelling the stochastic nature of the change in wind profile as it travels and optimizing feed-forward control for operation in the presence of the resulting measurement errors will be pivotal in realizing the anticipated performance improvement from preview control.

Currently, most control algorithms depend on measurements from turbine structure and drive train for use in the control feedback. Often these turbine measurements are unreliable or exhibit delayed response to disturbances acting on the turbine. This constrains the controls to react to complex atmospheric disturbances after their effects have been “felt” by the turbine. Thus, there is an inherent lag between the time that a disturbance arrives and the time that the control actuator begins to mitigate resulting loads. A considerable advantage in load mitigating capability can be attained by measuring atmospheric phenomena upwind of the turbine before

they impact the turbine rotor. The needed control actuation signals can then be prepared in advance and applied as the inflow to the turbine changes with potentially significant load mitigation improvement.

New lidar technologies are capable of measuring velocity upwind of the turbine with sample rates in the 10's of Hz. With these measurements, it is possible to design preview controllers that can adjust pitch (and/or torque) as necessary before wind disturbances arrive at the turbine. The preview control can be designed in unison with the feedback control or separately from feedback.

A plant augmented, preview controller is designed with the same techniques as used in the design of the MIMO controller of the previous section. The generalized plant approach extends so that a combined feedback and feed forward (preview) controller can be designed. The response of the resulting preview controller is displayed along with that of the PID/notch and MIMO, feedback controllers. As expected, the preview controller significantly improves performance without large increases in actuation.

The increasing awareness of the need for environmentally sustainable housing and cities has driven the promotion of wind energy conversion systems for the built environment.

One of the results of the development of solutions for the built environment is the re-appearance of vertical-axis wind turbines (VAWTs). In the built environment, the

VAWT presents several advantages over the more common horizontal-axis wind turbines, namely: its low sound emission (consequence of its operation at lower tip speed ratios), better aesthetics because of its three dimensionality, its insensitivity to yaw wind direction and its increased power output in skewed flow (see Martens *et al.*1 and Samoa Ferreira *et al.*2).

The phenomenon of dynamic stall is an inherent effect of the operation of a VAWT at low tip speed ratios.

The presence of dynamic stall has a significant impact on both loads and power. The unsteady variation in loads and the separation of the flow result in the release of large vortices into the flow, which consequentially interact with the airfoil.

The validation of dynamic stall simulations based on integral values such as load is usually impaired because: (i) the use of integral values can mask error cancellation, thus leading to incorrect simulations delivering results that, at first glance, seem feasible. (ii) Dynamic stall generates a random component on loads. For VAWTs in particular, the blade vortex interaction as the blade moves leeward leads to a high variability in loads. Code validation through integral values such as normal forces might yield ambiguous results because of this high variability.

The objective of the current work was to evaluate whether using particle image velocimetry (PIV) measurements of the shed vertical field can bring extra insight into the physics of the flow field and can be used as an additional validation parameter.

Modelling the VAWT in dynamic stall presents five immediate challenges in computational cost

- the unsteady component of the flow requires a time accurate model, adding an extra dimension (time) to the numerical grid.

- the geometry of the rotor does not allow for important spatial/time grid simplifications to be applied (e.g. moving reference frames or radial symmetry).

The movement of the airfoil implies an asymmetry between the conditions in the windward and in the leeward movement of the blade (in relation to wind direction). The low number of blades results in an instantaneous flow field that, at each azimuthally position, is significantly different from the time-averaged flow field.

- the large amount of shed vorticity implies that the model could be sensitive to numerical dissipation.

- the geometry of a VAWT results in blade–vortex interaction during the downwind passage of the blade, between the blade and the shed vorticity that was generated during the upwind passage. This implies that the development of the shed vorticity must be correctly modelled inside the entire rotor diameter; in order to avoid numerical dissipation, the spatial resolution of the grid must be very fine not only in the immediate vicinity of the blades but over the entire rotor.

- the variation of angle of attack of the blade with azimuth angle implies a varying relation/dominance between lift and drag force on the blade (resulting in instants during the rotation where the VAWT is actually being decelerated because only drag force is present). The correct use of a turbulence model and near-wall models is essential in these situations. This is particularly important at low tip speed ratios, where the power output of the VAWT is negative (for a certain range of λ); the performance at low tip speed ratios is highly important for start-up behaviour, one of the disadvantages usually associated with VAWTs.

The cost of direct numerical simulation of such a system renders it unfeasible, thus approximations of both turbulence and grid resolution must be made. The simulation and prediction of dynamic stall have been reviewed in Carr, which discussed the influence of parameters such as Reynolds numbers, transition, pitch rate and pitch axis location, amplitude and reduced frequency.

The dynamic stall behaviour of a VAWT is similar to and presents some of the same challenges as an airfoil pitching in large angles of attack, with the added complexity of the induction of the wake of previous rotations and the variation in perceived velocity during the windward/leeward movement of the blade.

Chapter5

Sliding Mode Control For Efficiency Optimization Of Wind Energy Systems With Double Output Induction Generator

5.1 Introduction

In recent years, there has been a growing interest in wind energy conversion systems (WECS) due to environmental, economical and political reasons and, consequently, many different WECS topologies have been developed. Among fixed-pitch grid-connected turbines, the induction machine is one of the most commonly used generating units (Ermis *et al.*, 1992; Smith, 1995). Moreover, despite a relative loss of reliability because of the presence of slip rings, double output induction generators (DOIG) have become an attractive alternative for grid-connected variable speed applications (Bose, 1986; Hadirci and Ermis, 1998; Salameh and Kazda, 1986; Ugitug *et al.*, 1994). The WECS with DOIG controlled through an AC/DC/AC rotor link has the following advantages:

- (1) The stator is directly connected to the grid, generating electricity at constant voltage and constant frequency in the presence of varying speed and load conditions (Hadirci and Ermis, 1992)
- (2) No exciter, neither voltage regulator nor synchronizer is required, so the weight of the generation system on the top of the turbine tower is diminished (Salameh and Kazda, 1986).
- (3) In this topology the generator can give more than its rated power because of the slip power recovery (Salameh and Kazda, 1986).
- (4) Compared with schemes controlled through stator converter, in these systems, converters are smaller and cheaper because they do not have to process total power, but only slip power
- (5) Compared with variable-pitch mechanical control systems, fixed pitch turbines completely controlled from the electrical side are more reliable and versatile.

. It has been established that variable speed WECS may extract more energy from the wind than constant speed systems. To achieve this goal, an appropriate control strategy is needed to track wind speed variations by adapting shaft speed and hence maintaining optimal energy generation. Owing to the nature of WECS, the controller has to be able to cope with nonlinear systems and model uncertainties.

Such attractive features can be obtained through sliding mode (SM) control. This control technique has proved to be very robust with respect to system parameter variations and external disturbances (Hung *et al.*, 1993). In addition, SM theory provides a simple designing procedure, even in the presence of a nonlinear model. The feasibility and benefits of SM control applied to electric drives have been previously shown in technical literature (Utkin, 1993). In this paper, a SM control strategy for generation efficiency maximization of wind-driven double output induction generator is proposed. In order to design the SM controller, an appropriate torque expression of the DOIG with slip power recovery is proposed. Then, conditions of maximum

energy generation are obtained and a SM control strategy for this type of variable-speed grid-connected WECS is developed.

5.2 Modelling of the DOIG with slip power recovery

The aim of this section is to introduce the electrical subsystem topology and to obtain a closed expression of the DOIG torque, suitable for SM designing purposes. The electrical subsystem of the WECS under consideration is a slip-power-controlled drive known as static Kramer drive (Figure 1). It consists of a DOIG and an electronic drive (ED), comprised by an uncontrolled bridge rectifier (C1), a line commutated inverter (C2) and a smoothing reactor (DC Link). In such configuration the stator power is directly fed to the grid while rotor power is partially recovered through the ED. The generator torque, and hence the system speed, can be controlled by modifying the "ring angle (α) of the inverter (ideally 90°) (Salameh and Kazda, 1986; Akpinar *et al.*, 1993):

The system is analysed under the following assumptions (Salameh and Kazda, 1986; Akpinar *et al.*, 1993):

- (1) Only the fundamental components are considered,
- (2) Ideal semiconductor devices,
- (3) The overlapping angle is neglected,
- (4) Saturation effects and core losses are neglected,
- (5) Balanced AC voltages are considered.

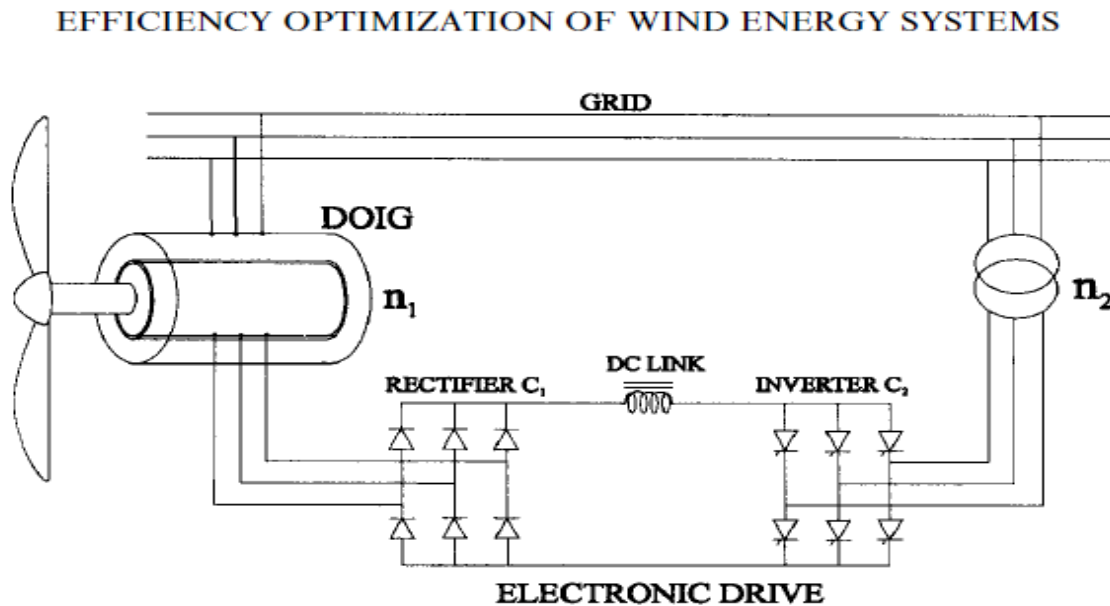


Figure 1. Electrical subsystem: DOIG with slip power recovery.

A sliding mode control for grid-connected variable-speed WECS with double output induction generator has been presented in this paper. The proposed strategy maximizes the characteristic robustness of sliding mode control by commanding the inverter "ring angle so that the extreme control values are maximized. Therefore, a very good tracking performance is obtained, even in the presence of external disturbances and model uncertainties. The prime control objective is maximum power generation, so generation efficiency of WECS with DOIG-ED has been analysed and conditions of generation efficiency optimization have been established. Besides, a closed expression of the DOIG-ED torque in function of the inverter "ring angle has been obtained. It has been proved to be adequate for the design of the sliding mode controller.

Finally, the effectiveness of the control facing simultaneously torque disturbances, un-modelled dynamics, parameter variations and grid voltage fluctuations has been demonstrated through computer simulation.

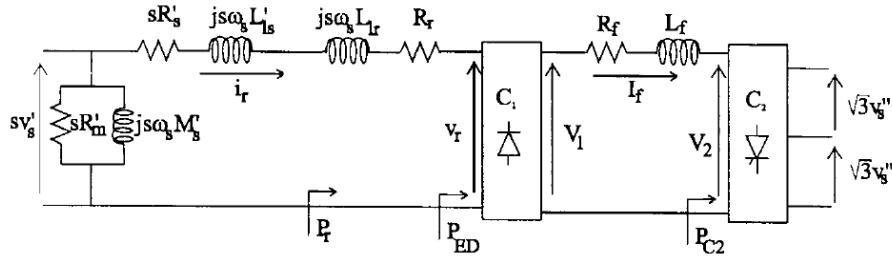


Figure 2. Per phase equivalent circuit of the DOIG referred to rotor, connected to the electronic drive.

To design the SM control strategy, an expression of the DOIG torque in function of α is needed. This goal will be accomplished with the help of the per phase equivalent circuit of the DOIG connected to the ED (Figure 2).

In that figure, v_s is the grid phase voltage and ω_s the synchronous electrical angular frequency. The slip is $s = (\Omega_s - \Omega)/\Omega_s$, with Ω the rotational speed, $\Omega_s = \omega_s/pp$ the synchronous rotational speed and pp the DOIG pair of poles. A single quotation mark applied to a stator variable indicates that it is referred to rotor windings by the stator/rotor turns ratio n_1 . On the other hand, quotation marks applied to voltage v_s indicate that it is referred to the C_2 terminals by the transformer turns ratio n_2 . Therefore,

$$V_s' = V_s/n_1 \quad (1)$$

$$V_s'' = V_s/n_2 \quad (2)$$

where V_s is the RMS value of the stator-phase voltage.

The DC voltages in terminals of C_1 and C_2 are

$$V_1 = 1.35\sqrt{3}V_r \quad (3)$$

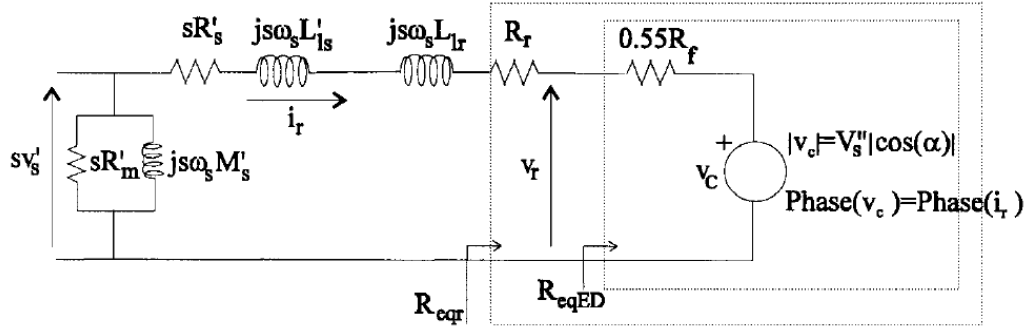


Figure 3. Per phase circuit of the electrical subsystem DOIG-DE referred to rotor.

$$V_2 = 1.35\sqrt{3}V_s''|\cos(\alpha)| \quad (4)$$

with V_r the RMS value of the fundamental component of the rotor voltage v_r .

The RMS value of the rotor phase current i_r is

$$I_r = \frac{\sqrt{6}}{\pi} I_f = 0.78I_f \quad (5)$$

with I_f the DC-Link current.

The slip power per phase results in

$$P_r = R_r I_r^2 + \frac{P_{EDtotal}}{3} = R_r I_r^2 + P_{ED} \quad (6)$$

where $P_{EDtotal}$ is the total power transferred from the rotor terminals to the ED, and P_{ED} represents such power per phase. A fraction of power $P_{EDtotal}$ is dissipated in the DC-Link resistance (R_r), while the rest (P_{C2}) is fed to the utility grid through inverter C_2 :

$$P_{EDtotal} = R_r I_r^2 + P_{C2} = R_r I_r^2 + V_2 I_f \quad (7)$$

Substituting Equations (4), (5) and (7) in Equation (6) yields

$$P_r = R_r I_r^2 + 0.55R_f I_r^2 + V_s''|\cos(\alpha)|I_r \quad (8)$$

Based on this equation, a per phase circuit of the electrical subsystem DOIG-ED can be presented (Figure 3). The ED is replaced by a resistance and a voltage source v_c , to represent the losses in the DC Link and the recovered power P_{C2} , respectively. According to Equation (8), the amplitude of v_c is a function of the firing angle of the inverter

$$\text{Amplitude}(v_c) = V_s''|\cos(\alpha)| \quad (9)$$

It is important to note that C_1 is an uncontrolled rectifier, thus the fundamental components of the rotor terminal voltage v_r and the rotor current i_r are in phase. This imposes the phase of source v_c to be

$$\text{Phase}(v_c) = \text{Phase}(i_r) \quad (10)$$

The power distribution in the electrical subsystem can be analysed with the help of the equations previously obtained. The expressions of the per phase mechanical power and the per phase air-gap power are similar to those of the short-circuited rotor induction generator, that is $P_m = T_g \Omega / 3$ and $P_e = T_g \Omega_s / 3$, respectively (Bose, 1986). On the other hand, according to (8), the per phase rotor power can be partitioned into the following per phase powers: dissipated in the rotor windings (P_{R_r}), dissipated in the DC Link ($P_{R_f} / 3$), and fed to the grid ($P_{C_2} / 3$).

Therefore, the ED can be treated as an external resistance R_{eqED} , function of α , and consequently the total equivalent resistance of the rotor circuit (R_{eqr}) results in

$$R_{\text{eqr}} = R_r + R_{\text{eqED}} = R_r + 0.55R_f + \frac{V_s'' |\cos(\alpha)|}{I_r} \quad (11)$$

In this way, the induction generator torque

$$T_g = \frac{-3V_s'^2 s R_{\text{eqr}}}{\Omega_s [(sR_s' + R_{\text{eqr}})^2 + (s\omega_s L_{1s}' + s\omega_s L_{1r})^2]} \quad (12)$$

can be adjusted by controlling the firing angle of the inverter. Note that in Equation (12) the induction machine torque is positive for generator operation and negative for motor action.

To obtain the expression of T_g in function of α , required for the design of the SM controller, it is necessary to eliminate I_r from Equation (11). The equation of I_r is

$$I_r = \frac{sV_s'}{\sqrt{(sR_s' + R_{\text{eqr}})^2 + (s\omega_s L_{1s}' + s\omega_s L_{1r})^2}} \quad (13)$$

From Equations (11) and (13), two solutions for R_{eqr} in function of α , are obtained:

$$R_{\text{eqr1}} = \frac{s[n_2^2 s R_b + (n_1 |\cos(\alpha)|)^2 R_s' - n_1 |\cos(\alpha)| \sqrt{\Gamma}]}{((n_2 s)^2 - (n_1 |\cos(\alpha)|)^2)} \quad (14)$$

$$R_{\text{eqr2}} = \frac{s[n_2^2 s R_b + (n_1 |\cos(\alpha)|)^2 R_s' + n_1 |\cos(\alpha)| \sqrt{\Gamma}]}{((n_2 s)^2 - (n_1 |\cos(\alpha)|)^2)} \quad (15)$$

with

$$R_b = R_r + 0.55R_f$$

$$\Gamma = 2n_2^2 R_b s R_s' + (n_2 s R_s')^2 + n_2^2 (s\omega_s L_{1s}' + s\omega_s L_{1r})^2 + (n_2 R_b)^2 - [n_1 |\cos(\alpha)| (\omega_s L_{1s}' + \omega_s L_{1r})]^2$$

Each one of these solutions corresponds to generator or motor operation of the double output induction machine (see Figure 4). It can be determined that

$$T_g \begin{cases} T_g(R_{\text{eqr1}}) & \text{if } \Omega \geq \Omega_s \text{ and } T_g \geq 0: \text{ Generator} \\ T_g(R_{\text{eqr2}}) & \text{if } \Omega \leq \Omega_s \text{ and } T_g \leq 0: \text{ Motor} \\ 0 & \text{else} \end{cases} \quad (16)$$

Note that points $T_g = 0$ in Figure 4 occur when $V_1 < V_2$ and then the diodes of C_1 are reverse biased ($i_r = 0$). The rotor current reappears, and consequently the electromagnetic torque, when $|s|$ (in super or subsynchronous operation) is big enough to induce a voltage in the rotor windings such that $V_r > V_s$.

For a better interpretation, the power distribution is depicted in the T/Ω plane (Figure 5). As a first case study, a constant driving torque and a fixed firing angle $\alpha = 90^\circ$ is considered. Under these conditions, the system operates at point A (see Figure 5(a)). Given that $|\cos(\alpha)| = 0$, in this case, no slip power is recovered ($P_{C2} = 0$) and hence, the presence of the ED merely appears as an increment of the rotor resistance (this can be observed in Figure 5(a) as a reduction in the slope of the T_g characteristic, if it is compared with the characteristic of the DOIG without ED and short-circuited rotor terminals).

The power dissipated in the rotor windings and dissipated in the DC Link are represented by areas I and II, respectively, and are directly proportional to the values of R_r and $0.55R_r$. The division between areas I and II can be graphically obtained from the intersection point between the driving torque and the T_g characteristic of the DOIG without ED (point B in Figure 5(a)). That is because, in short-circuited rotor induction generators, all the slip power is dissipated in R_r (Area II in Figure 5(a)). The total air-gap power is represented by Area III, which, neglecting stator and core losses, also corresponds to the stator generated power. Finally, the total mechanical power results from the union of areas I-III.

If α increases and the driving torque remains constant, the system operation point shifts to C (see Figure 5(b)). Because of the constant driving torque, the total dissipated power ($P_{R_r} = \text{Area I}$ and $P_{R_r, \text{total}} = \text{Area II}$) and the stator generated power ($P_{e, \text{total}} = \text{Area III}$), have not changed with respect to those of the previous case ($\alpha = 90^\circ$). However, the total mechanical power has augmented ($\text{Area I} + \text{II} + \text{III} + \text{IV}$). Therefore, the power increase (Area IV) corresponds to the recovered slip power P_{C2} . Area IV is determined by the crossing point Ω_1 . It is a function of α and can be obtained by doing $T_g = 0$ in (16)

$$\Omega_1 = \Omega_s \left(1 + |\cos(\alpha)| \frac{n_1}{n_2} \right)$$

EFFICIENCY OPTIMIZATION OF WIND ENERGY SYSTEMS

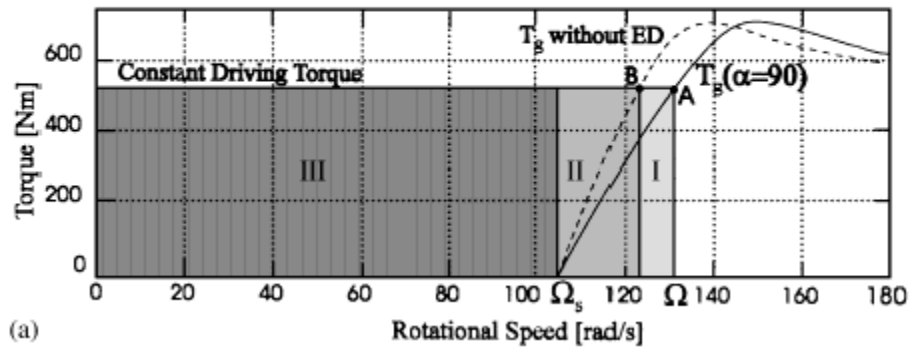
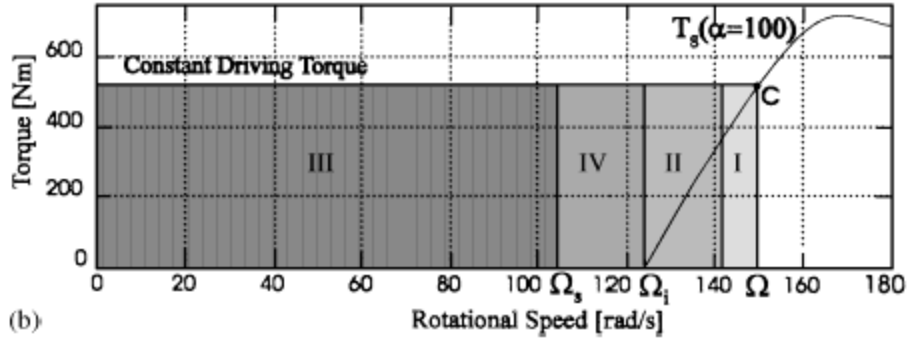


Figure 5(a). Power distribution with $\alpha = 90^\circ$: $P_{R_r} = \text{Area I}$, $P_{R_r, \text{total}} = \text{Area II}$, $P_{e, \text{total}} = \text{Area III}$, $P_{m, \text{total}} = \text{Area (I + II + III)}$ and $P_{C2} = 0$. In dashed line: T_g characteristic of the DOIG with short-circuited rotor terminals.



(b). Power distribution with $\alpha = 100^\circ$: $P_{R_f} = \text{Area I}$, $P_{R_f, \text{total}} = \text{Area II}$, $P_{e, \text{total}} = \text{Area III}$, $P_{C2} = \text{Area IV}$. $P_{m, \text{total}} = \text{Area (I + II + III + IV)}$ and $P_{\text{gen}} = \text{Area (III + IV)}$.

5.3 Conclusion

The proposed strategy maximizes the characteristic robustness of sliding mode control by commanding the inverter firing angle so that the extreme control values are maximized. Therefore, a very good model tracking performance is obtained, even in presence of external disturbances and model uncertainties. The prime control objective is maximum power generation, so generation efficiency of WECS with DOIG-ED has been analysed and conditions of generation efficiency optimization have been established. Besides, a closed expression of the DOIG-ED torque in function of the inverter firing angle has been obtained. It has been proved to be adequate for the design of the sliding mode controller. Finally, the effectiveness of the control facing simultaneously torque disturbances, unmodelled dynamics, parameter variation and grid voltage fluctuations has been demonstrated through computer simulation.

CHAPTER 6

Simulating Dynamic Stall in a Two-Dimensional Vertical-Axis wind turbine (VAWT)

6.1 Introduction

The increasing awareness of the need for environmentally sustainable housing and cities has driven the promotion of wind energy conversion systems for the built environment.

One of the results of the development of solutions for the built environment is the re-appearance of vertical-axis wind turbines (VAWTs). In the built environment, the VAWT presents several advantages over the more common horizontal-axis wind turbines, namely: its low sound emission (consequence of its operation at lower tip speed ratios), better aesthetics because of its three dimensionality, its insensitivity to yaw wind direction and Copyright c 2009 John Wiley & Sons, Ltd. **1** its increased power output in skewed flow.

The phenomenon of dynamic stall is an inherent effect of the operation of a VAWT at low tip speed ratios (1). The presence of dynamic stall has a significant impact on both loads and power. The unsteady variation in loads and the separation of the flow result in the release of large vortices into the flow, which consequentially interact with the airfoil.

- The variation between the points of maximum value of angle of attack, dynamic pressure and lift for the upwind blade, and their corresponding values for the downwind passage, occurs as a faster process in the leeward movement ($q = 90^\circ$ to $q = 270^\circ$) of the blade than in the windward movement of the blade ($q = 270^\circ$ to $q = 90^\circ$.)
- another source of unsteadiness is the blade vortex interaction that occurs not only in the downwind passage, but also during all the leeward movement of the blade; the near wake of the blade generated in the upwind passage is convected with the blade in the leeward movement.
- The shedding of strong, discrete, separated leading-edge vortices, travelling over the upper surface and the trailing edge, will result in fast oscillations of the pressure field and force around the blade.

investigation of pitchable VAWTs in ground effect 16 re-designed for the PIV experimental work.

The large aspect ratio of the blade ($AR = 20$) and the use of two symmetry disks at the blade tips achieve 2-D flow conditions at the midsection. The computational fluid dynamics (CFD) model simulates the aerodynamics at the midsectio

6.2 Motion and aerodynamics of A VAWT

The movement of the blades in a VAWT entails a variation of tangential and normal velocity perceived by the blade, resulting in a varying angle of attack and dynamic pressure (figure 1). At low tip speed ratios ($\lambda < 4$), the angle of attack of the blade can exceed the static stall angle ((figure 2), and this, in the case of unsteady flow, can result in dynamic stall.

The level of unsteadiness is determined by the reduced frequency k , which was for this experimental work $k = 0.125$, placing the work in the unsteady aerodynamics region. The reduced frequency k is defined as $k = w.c/2V$, where w is the angular frequency of the unsteadiness, c is the blade's chord and V is the velocity of the blade. In this experiment, because of the variation of V with rotation angle, k was defined for a VAWT as $k = w.c/(2.1.U_\infty) = w.c/(2.w.R) = c/(2.R)$, where $\lambda = w.R/U_\infty$ is the tip speed ratio and R is the radius of the turbine. The frequency of the unsteadiness is the same as the rotational frequency, assuming that the main source of unsteadiness is the variation of angle of attack and dynamic pressure. This assumption, although generally correct, does not take into account several factors, namely:

- The variation between the points of maximum value of angle of attack, dynamic pressure and lift for the upwind blade, and their corresponding values for the downwind passage, occurs as a faster process in the leeward movement ($q = 90^\circ$ to $q = 270^\circ$) of the blade than in the windward movement of the blade ($q = 270^\circ$ to $q = 90^\circ$); it is possible to say that the reduced frequency is in fact varying during the rotation.

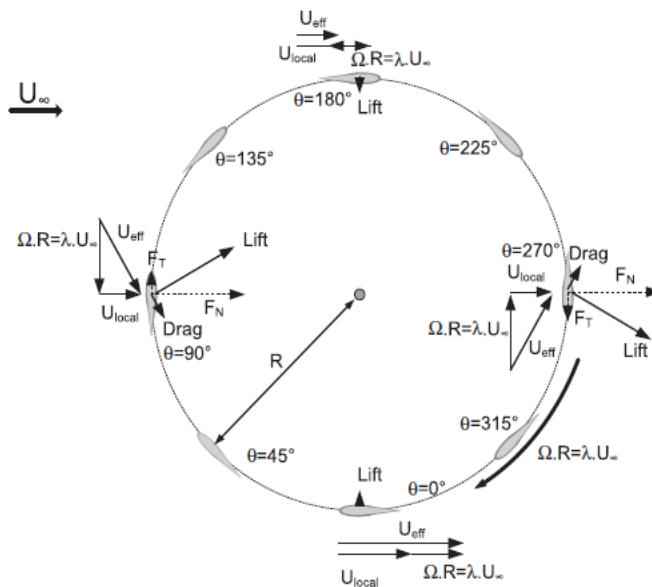


Figure 1. Schematic of the rotation of a VAWT at eight azimuthal positions; the scheme represents the effective velocity U_{eff} perceived by the blade at $\theta = 0^\circ, 90^\circ, 180^\circ$ and 270° , and the resultant orientation of the lift-and-drag forces and their decomposition in normal F_N and tangential F_T forces.

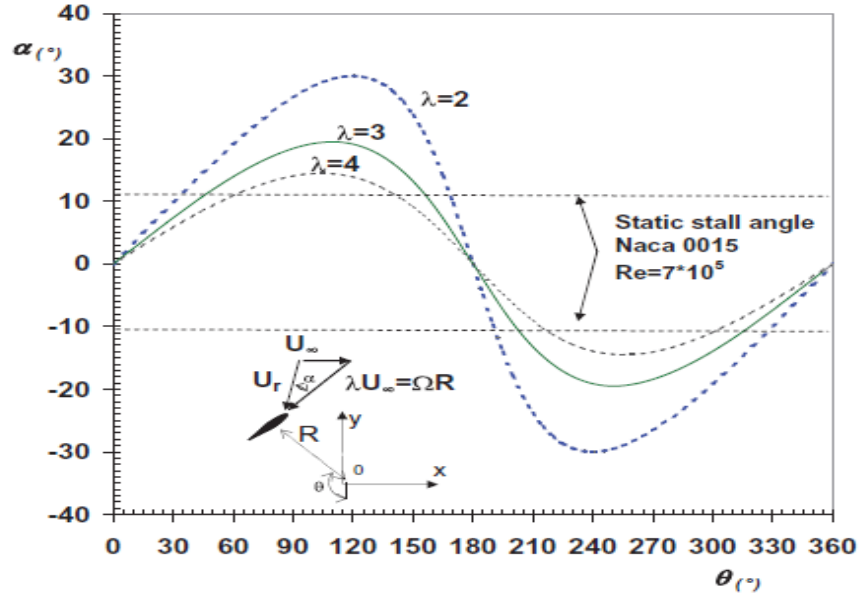


Figure 2. Plot of the angle of attack perceived by the blade (no effect of induction included) for $\lambda = 2, 3$ and 4 ; the curves are plotted in comparison to the static stall angle at similar Re for a $N_{ACA}0015$.

- another source of unsteadiness is the blade vortex interaction that occurs not only in the downwind passage, but also during all the leeward movement of the blade; the near wake of the blade generated in the upwind passage is convected with the blade in the leeward movement. Yet, the variation of the strength of the shed wake means that the blade vortex interaction will occur with discrete, strong vortices, resulting in faster oscillations of force.
- the shedding of strong, discrete, separated leading edge vortices, travelling over the upper surface and the trailing edge, will result in fast oscillations of the pressure field and force around the blade.

6.3 Simulation definition

6.3.1 Model geometry

The geometry of the model is a two-dimensional (2-D) representation of the experimental setup in Simão Ferreira *et al.*⁷ The experimental setting consists of an H-VAWT initially built for the investigation of patchable VAWTs in ground effect, 16 re-designed for the PIV experimental work. The large aspect ratio of the blade ($AR = 20$) and the use of two symmetry disks at the blade tips achieve 2-D flow conditions at the midsection. The computational fluid dynamics (CFD) model simulates the aerodynamics at the midsection.

The model is bounded by two walls spaced 1.25 m apart, where a 0.4 m diameter single-bladed VAWT is placed. All walls are defined as a non-slip boundary condition.

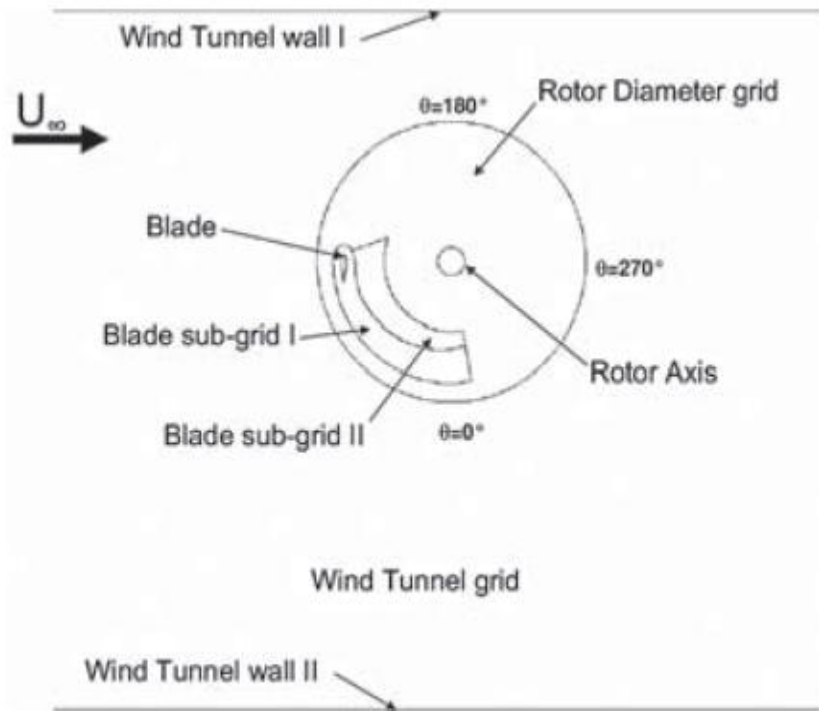


Figure 3. Diagram of the model geometry, subgrid distribution and wall boundaries.

The CFD grid presents a discrepancy (15% chord) in the location of the airfoil in tangential direction used in the experiment, only identified after most of the calculations were completed. The difference in location of the pitching axis of the airfoil leads to a difference in the added circulation caused by a constant pitching motion. This added circulation caused by pitching is proportional to tip speed ratio, rotor solidity and the location of the pitching axis.

Despite the large rotor solidity, taking into account the low tip speed ratio of the simulation and the small discrepancy in location of the pitching axis, further calculations showed this added circulation to be small when compared with the circulation caused by angle of attack, and negligible for the current validation of the results and its implications.

14*D* downwind of the rotor respectively allowing a full development of the wake.

The CFD grid presents a discrepancy (15% chord) in the location of the airfoil in tangential direction used in the experiment, only identified after most of the calculations were completed. The difference in location of the pitching axis of the airfoil leads to a difference in the added circulation caused by a constant pitching motion. This added circulation caused by pitching is proportional to tip speed ratio, rotor solidity and the location of the pitching axis.

Despite the large rotor solidity, taking into account the low tip speed ratio of the simulation and the small discrepancy in location of the pitching axis, further calculations showed this added circulation to be small when compared with the circulation caused by angle of attack, and negligible for the current validation of the results and its implications.

The model thus represents accurately the geometric conditions of the midsection of the experiment. The rotor is represented by a 0.05 m chord *NACA0015* airfoil and the 0.05 m rotor axis. The rotor axis is placed at a distance of 0.80 m from the lower wall, as in the experimental setting. The inlet and outlet boundary conditions are placed 10*D* upwind and 14*D* downwind of the rotor, respectively, allowing a full development of the wake.

6.3.2 Computational space grid

The grid is composed of four non-conformal sub grids rotor diameter, blade sub grid I, blade sub grid II and wind tunnel, each a structured grid of quadrilateral elements. The shape and location of each sub grid, and the wall boundary conditions representing the airfoil/blade, wind tunnel walls and rotor axis (the flow inlet and outlet boundary conditions are not represented).

Blade sub grid I covers the region of the airfoil and trailing edge near wake. Blade sub grid II is a refined region of the remaining rotor diameter, aiming at capturing the development of the released and convected leading-edge tip vortex, as well as the roll-up region of leading-edge and trailing edge separated vortices during the leeward movement of the blade. The rotor diameter grid covers the remaining region, with a radius 1.25*R*. The wind tunnel grid represents all the regions outside the 1.25*R* area.

The use of moving sub grids is necessary because of the movement of the rotor elements. Thus, the sub grids rotor diameter, blade sub grid I and blade sub grid II rotate with an angular velocity ω , while the sub grid wind tunnel remains fixed. The option of dividing the rotor space into three non-conformal sub grids allows the use of a structured grid without compromising its quality or requiring a large mesh with excessive refinement in areas of lower importance.

A quadrilateral structured grid also allows easier control of the refinement of the grid; this aspect is crucial in the present work, since the sensitivity to the refinement of the space grid is evaluated

.the most refined sub grid is blade sub grid I that defines the geometry of the airfoil and its immediate wake development flow region. The reference fine grid comprises 3305 nodes over the airfoil surface, where the height of the first row of cells is set at a distance from the wall of $0.02\%c$ (equivalent to a value for the viscous sub layer scale $y^+ \approx 1$ when $q = 90^\circ$ for $k - \epsilon$ model). The total model (the four sub grids) size comprises approx. 1.6×10^6 cells.

6.3.3 Simulated flow conditions

The simulation aimed at representing the flow conditions of the experimental work for $l = 2$ and incoming flow $U_\infty = 7.5 \text{ m s}^{-1}$, resulting $w = 75 \text{ rad s}^{-1}$. Because of the importance of the induction of the rotor, it is necessary to perform a simulation for several rotations until a fully developed wake is present. All values presented in this paper relate to the revolutions of the rotor after a periodic, post-transient solution is attained.

6.4 Validation of the results of different turbulence models

Four different turbulence models were used in this work: two unsteady Reynolds-averaged Navier–Stokes (URANS), Spalart–Allmaras (S–A) and $k - \epsilon$, and two large eddy models, detached eddy simulation (DES) and large eddy simulation (LES). All simulations have been implemented in Fluent. The S–A used is the implementation in the CFD package¹⁷ of the model proposed in Spalart and Almaras.¹⁸ The $k - \epsilon$ model is the standard implementation referred to as RNG $k - \epsilon$.

The LES and DES used are the standard models implemented for 2-D/three-dimensional (3 D) simulations. The simulation results are validated against the experimental results in Simão Ferreira *et al.*⁷ for the case of $l = 2$.

Figures 4 and 5 are an example of these results, showing, respectively, the evolution of leading-edge and trailing-edge vorticity at different moments of the rotation. The flow is characterized by the shedding of strong vortices, located: (i) at the leading edge, resulting from leading-edge separation where the clockwise vortices detach from the surface; and (ii) at the trailing edge, where a wake is formed from the pressure side boundary layer and the boundary layer developed on the suction side, aft of the re-attachment point of the separated leading-edge flow; this wake is formed at the trailing edge of the airfoil by the adding of the two boundary layers, experiencing a roll up because of the strong vorticity. The validation of the simulations compares the vorticity field in the vicinity of the airfoil at azimuthal angles of $q = 90^\circ$ and $q = 120^\circ$; the choice of these two moments of the rotation is driven by the development of the vorticity shed from the leading edge and the development of the wake at the trailing edge.

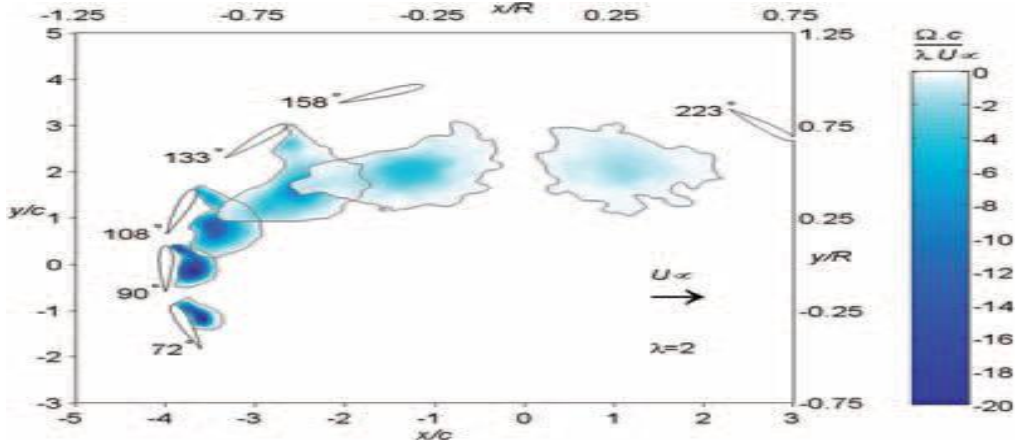


figure 4. PIV experimental data of the evolution of the circulation of leading-edge separated vortex for $\lambda = 2$ at 90° , 108° , 133° and 158° .

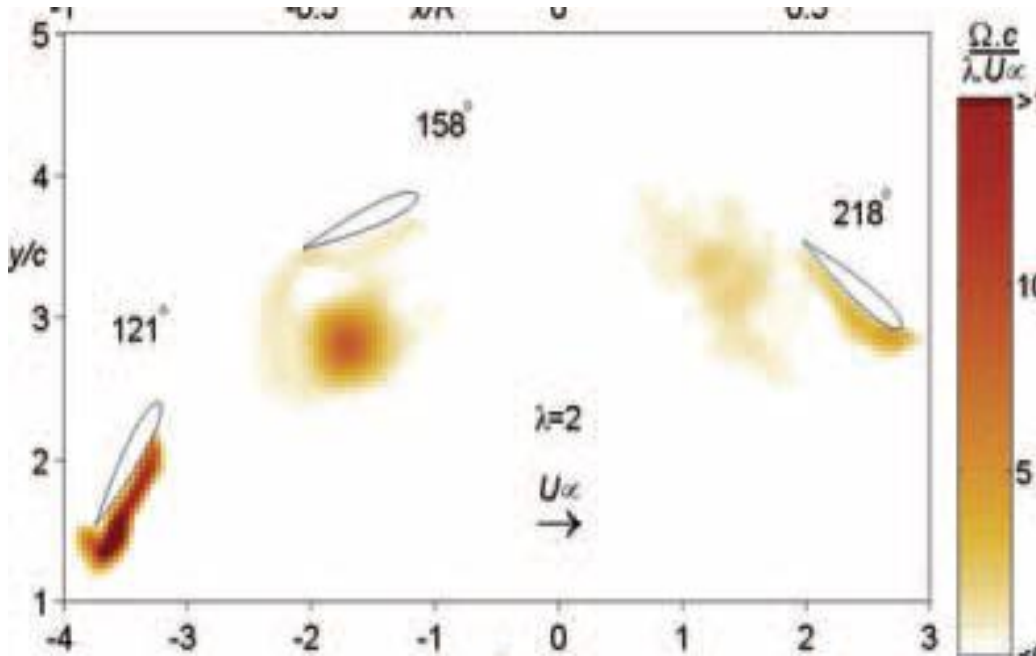


figure 5. PIV experimental data of the evolution of the counter-clockwise vorticity shed after the roll-up of the trailing-edge vorticity⁷

The validation of the simulations compares the vorticity field in the vicinity of the airfoil at azimuthal angles of $q = 90^\circ$ and $q = 120^\circ$; the choice of these two moments of the rotation is driven by the development of the vorticity shed from the leading edge and the development of the wake at the trailing edge

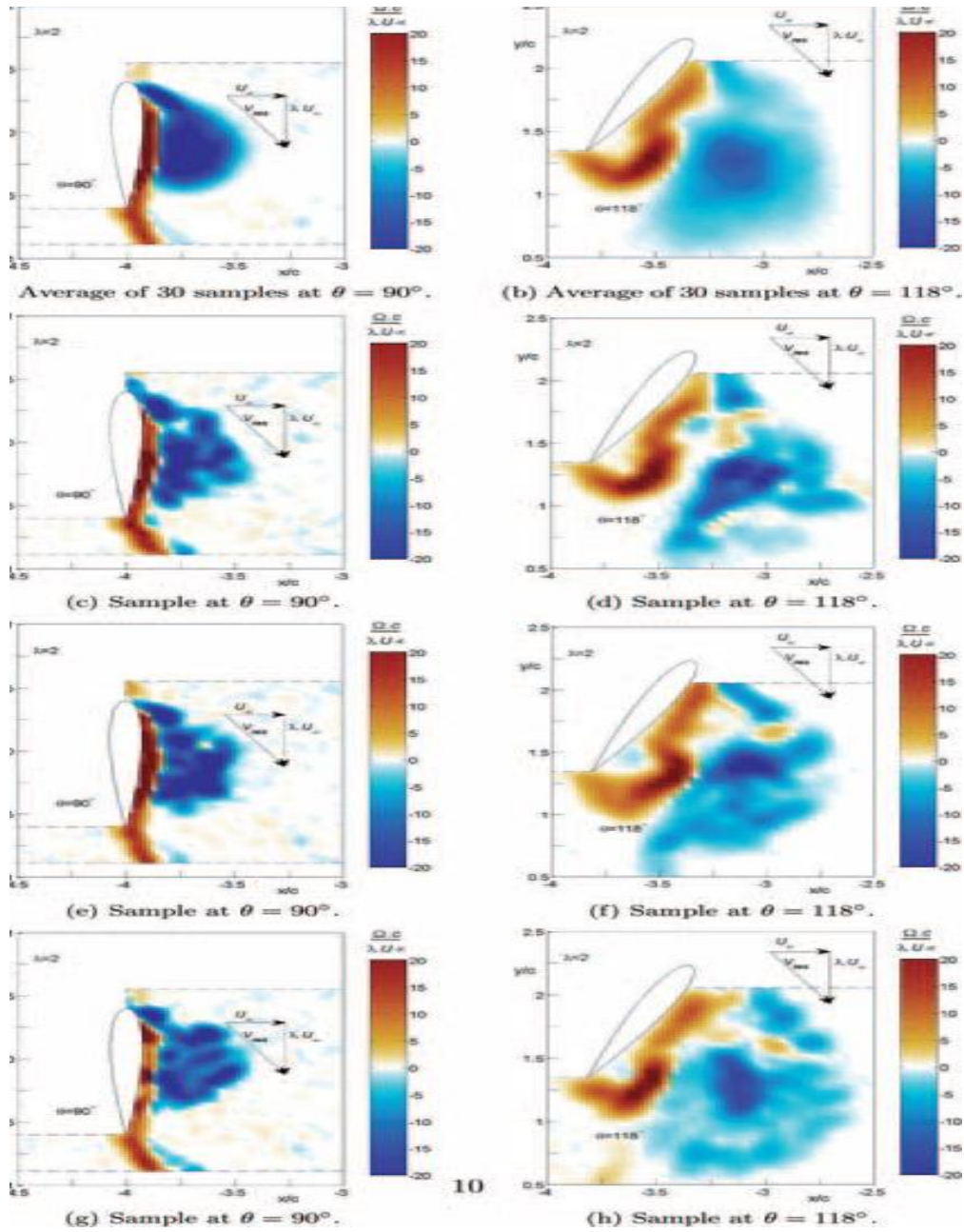


Figure 6. Experimental PIV result of vorticity field for $\theta = 90^\circ$ and $\theta = 118^\circ$; phase average and instantaneous samples

Figure 6 above shows the experimentally measured vorticity field for $q = 90^\circ$ and $q = 118^\circ$, both the 30-sample phase locked average and three individual samples for each angle. The individual samples show that the vorticity shed

6.4.1 URANS models (unsteady Reynolds-averaged Navier–Stokes)

Some previous attempts at simulating 2-D VAWT flow (see Hansen and Sørensen,¹⁰ Allet *et al.*,¹¹ Paraschivoiu and Allet,¹² Paraschivoiu and Béguier¹³ and Paraschivoiu¹⁴) have resorted to these or similar models; the results presented in this paper using URANS are thus a link between that previous research and the application of more complex models such as LES and DES.

Figure 7(a),(b) shows the computed vorticity field in the vicinity of the airfoil at $q = 90^\circ$ and $q = 120^\circ$. Compared with the experimental results (Figure 6), the S–A model underestimates the generation and shedding of vorticity at the leading edge (in the simulation, the leading-edge shed vorticity is only located in the first half of the airfoil, while experimental results show it covering the entire airfoil length; Figures 4 and 6). The simulation also fails to predict the roll-up of the trailing-edge shed vorticity clearly seen in the experimental work (Figures 5 and 6) even at $q = 120^\circ$.

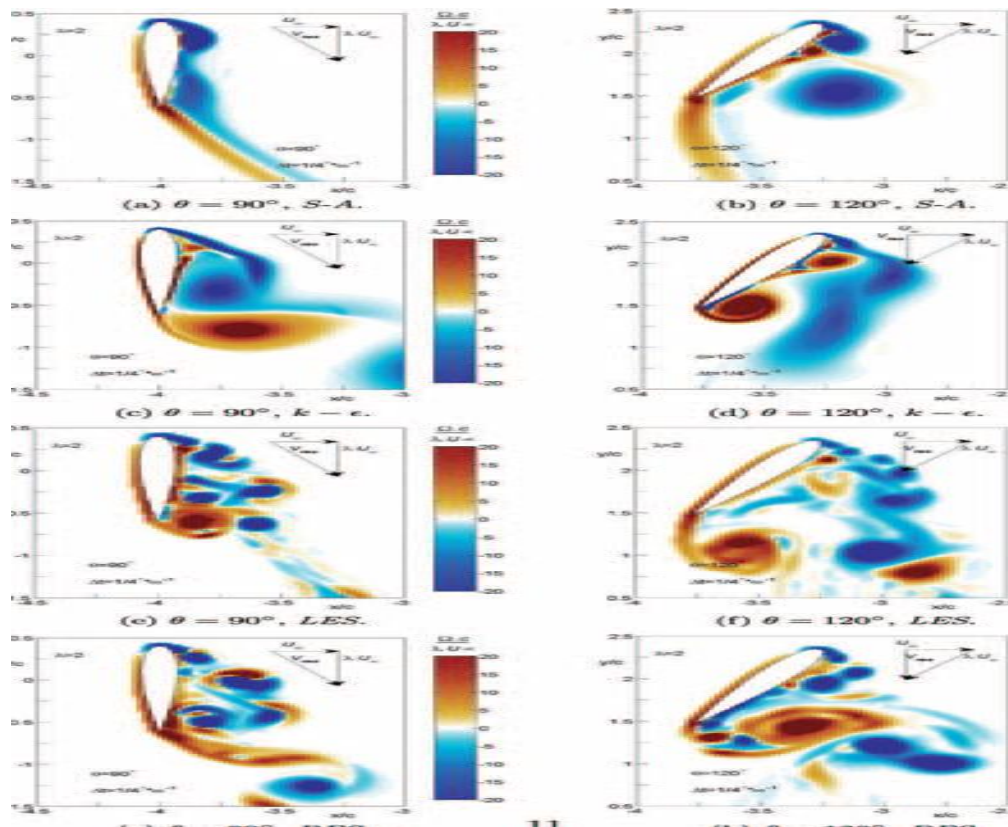


Figure 7. Vorticity field for $\theta = 90^\circ$ and $\theta = 120^\circ$, four turbulence models

6.4.2 LES (large eddy simulation)

Contrary to URANS, in LES the equations are not Reynolds averaged in time, but are space filtered (averaged in volume). This operation implies an increase of the computational requirements, but reduces the turbulence modelling to only the sub-grid scale (SGS model), directly solving the N-S equations for the larger scales of turbulence.

The application of a 2-D formulation of the LES and DES models is clearly inferior to a 3-D formulation, which can model the three-dimensionality of the separated vertical structures. Comparisons between 2-D and 3-D formulations of LES for the simulation of unsteady flows with large vertical structures have shown distinct results regarding the suitability of the 2-D formulation, and its performance in comparison with the 3-D formulation.

6.4.3 DES (detached eddy simulation)

DES is a hybrid method of LES and URANS, where the wall region is modelled with a URANS model and the outer region with LES; the motivation for using DES is the high cost of LES in the boundary layer region; the strategy of using DES aims at still accurately model the large vortices in the separated shed wake, while keeping the simulation of the near-wall region at a limited cost. In the present work, an S-A model is used for the wall region.

Of all the models used, the DES simulations present the results best agreeing with experiments in Figure 6; the region and location of the vorticity, and specially the phase of roll-up of the trailing- edge wake at $q = 90^\circ$ are as experimentally observed. The distribution of small concentrated vortices in the DES model resembles that observed in the instantaneous samples in Figure 6 above in contrast to the continuous smooth distribution of vorticity predicted by the $k - \epsilon$ model.

6.5 Comparison of force simulation

vorticity with experimental observations. The values of tangential and normal forces* will now be compared.

Three main differences are visible between the URANS models and the large eddy models DES and LES: The models have until now been analyzed by comparing only the evolution of the shed

- A large value of normal force at $q = 0$ for both URANS models (lower in the $k - \epsilon$ model), representing a large value of lift at a zero geometric angle of attack; in both the DES and LES

Models, the value of the force is positive but low, as observed in previous experimental work and simulations.

- the azimuthal location of the maxima of tangential and normal forces: in the DES and LES models, both tangential and normal forces reach a maximum at lower values of q (in comparison with the URANS models),

followed by an almost linear decrease with q . The cause for the different evolution of force in the URANS models might lie on their inability to correctly model the development of vorticity around the airfoil.

- the level of unsteadiness of the forces; the DES and LES present large oscillations in the forces at frequencies higher than the frequency of rotation of the turbine. This might be a result of the shedding of strong small vortices in the DES and LES as opposed to a single continuous vortex in the URANS models.

However, numerical convergence effects might also be in the origin of these fluctuations. The results of the URANS $k - \epsilon$ model show a large, phase-locked oscillation at $q = 90^\circ$ to $q = 110^\circ$, which is consistent with the interaction of one single large leading-edge vortex with one large trailing-edge vortex, as seen in Figure 7 above. In the DES model, the vorticity is distributed in smaller vortices, resulting in a smoother variation in loads. This comparison shows the impact of the correct modelling of the shed wake in load fluctuations.

6.6 Verification of grid sensitivity

In this section, we shall evaluate the robustness of the DES simulation with respect to time step and grid refinement.

6.6.1 Time step refinement

In the reference simulation, a time step $\Delta t = 1/4^\circ w^{-1}$ is used. The analysis now presented compares this simulation with two others with the same initial conditions but time steps $\Delta t = 1/8^\circ w^{-1}$ and $\Delta t = 1/16^\circ w^{-1}$. The figure (9) and (10) present the vorticity distribution at $q = 90^\circ$. For the DES model, the first refinement of the time step ($\Delta t = 1/8^\circ w^{-1}$) results in an over-generation of the vorticity and an early roll-up of the wake at the trailing edge. Yet, the second refinement ($\Delta t = 1/16^\circ w^{-1}$) does not result in greater over-generation; in fact, the differences between the two results ($\Delta t = 1/8^\circ w^{-1}$ and $\Delta t = 1/16^\circ w^{-1}$) are minimal and in what might be expected in relation to the randomness of the flow. This interpretation of the results is also confirmed by the simulated force values. The DES simulation appears (despite the limited time step sensitivity analysis) to have a low sensitivity to time step refinement at this magnitude of step size. For $q > 100^\circ$, the two simulations with smaller time step converge to similar values; this result emphasizes the relevance of convergence effects on the development of the solution for $q > 100^\circ$, where blade-vortex interaction is dominant.

6.6.2 Space grid refinement

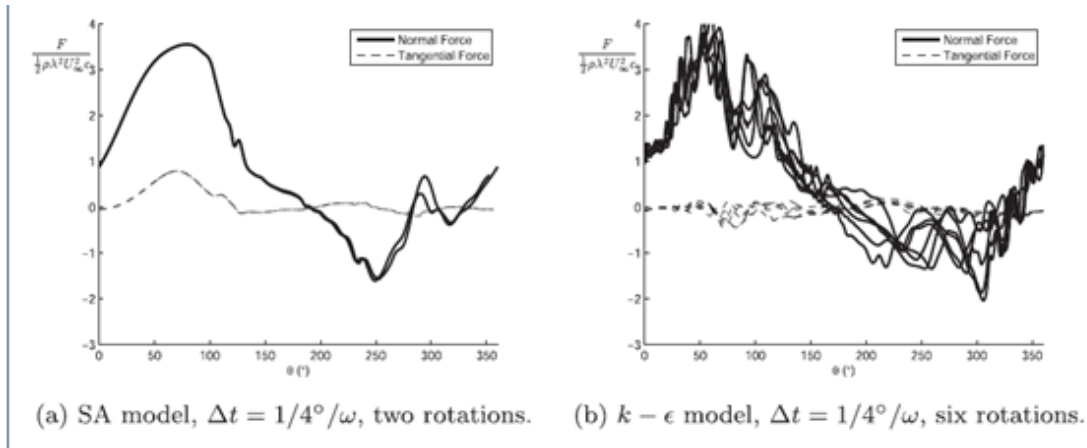
Two simulations were performed with coarser space meshes (x and y); only blade sub grid I was coarsened, in the first case by quadrupling the cell area ($4\Delta A$, doubling height and width) and in the second case by 16-fold ($16\Delta A$, quadrupling height and width).

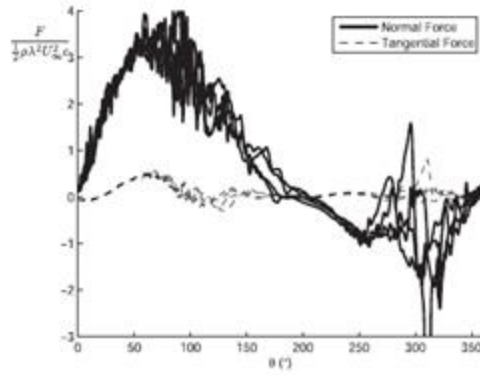
The results show the over generation of vorticity in comparison with the experimental results; this over-generation also occurs when using the DES model; however, the effect on the force is small. For $q < 180^\circ$, the force distributions for the different space grid resolutions follow the same trend and mostly overlap; for $q > 180^\circ$, when the airfoil is once again interacting with the shed vorticity from the upwind passage, the randomness of the solution is too large to make any comment on the impact of grid resolution. The current simulations do not allow to estimate if the three different solutions (for the three different grid resolutions) are a result of the impact of grid resolution of the solution when $q > 180^\circ$, or just a cumulative numerical effect of the solution; in the latter case, an increasing refinement of the spatial grid will not bring any further accuracy.

6.7 Verifying high- frequency variation in force

As mentioned before, the oscillations observed in the force output at frequencies much higher than the rotational frequency can have two origins: (i) a numerical convergence problem, where for each time step, the solution converges slightly faster or slower, thus undershooting or overshooting the real value; and (ii) a real physical behaviour resulting from the continuous shedding of strong small vortices over the surface and at the trailing edge.

* Tangential force is considered in the direction of rotation of the blade and normal force in the radial direction.





(c) LES model, $\Delta t = 1/4^\circ/\omega$, four rotations.

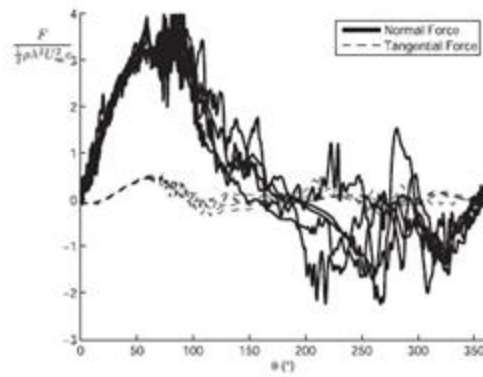


Figure 8 (c) ,(d)

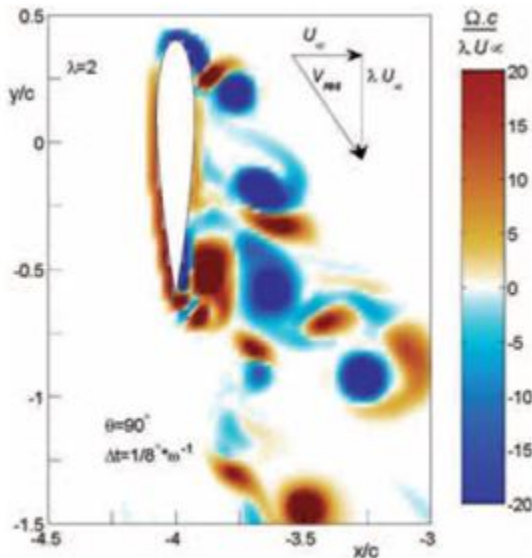


Figure 9. Vorticity field at $\theta = 90^\circ$, $\Delta t = 1/8^\circ\omega^{-1}$.

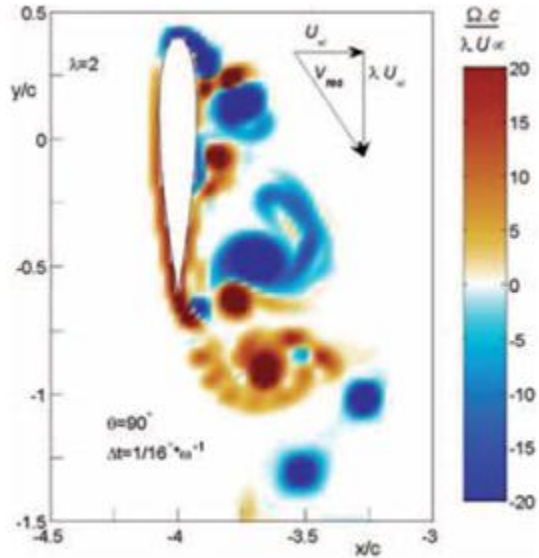


Figure 10. Vorticity field at $\theta = 90^\circ$, $\Delta t = 1/16^\circ\omega^{-1}$.

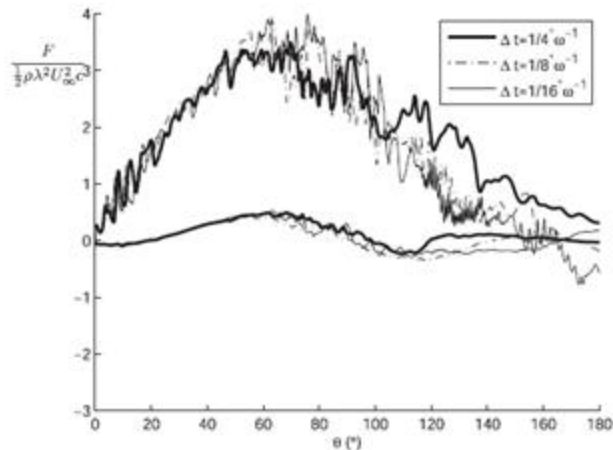


Figure 11. Effect on tangential and normal force of change of the time grid refinement.

To observe the validity of the former, three simulations of a half rotation of the rotor, starting at the same initial condition, are compared. The three solutions encompass: (i) the reference model, with $\Delta t = 1/4^\circ\omega^{-1}$ and N iterations per time step; (ii) a second model, with $\Delta t = 1/4^\circ\omega^{-1}$ and $2N$ iterations per time step; and (iii) a time refined model, with $\Delta t = 1/8^\circ\omega^{-1}$ and N iterations per time step.

The results do not present any large change on the amount of high-frequency oscillations on the force curve, with the main difference between the curves occurring past the roll-up of the trailing-edge vorticity at $q > 90^\circ$. The evolution of percentiles of the iterative convergence of the force on the airfoil. The force solutions tend to converge (<0.01) for iteration numbers between 40 and 80. Thus, although convergence can account for some of the magnitude of the oscillations in force, it is not the main source for the region of $q < 90^\circ$. For $q > 90^\circ$, the blade-vortex interaction becomes dominant, and the effect of convergence may be even more relevant, creating an artificial randomness to the flow.

6.8 Conclusion

These results demonstrate the influence of different turbulence models on the accuracy of the prediction of dynamic stall development on a VAWT. Of the models analyzed, the DES turbulence model resulted in predictions that most closely matched the experiments.

The DES model is not only able to predict the generation and shedding of vorticity and its convection, it also shows an acceptable sensitivity to grid refinement (both space and time), thus making it suitable for simulations where validation data are limited or non-existent.

URANS models proved insufficient because of their inability to correctly model the large eddies, and the influence of this in the development of forces in the downwind passage of the rotor. The

LES performed worse than the DES model, probably because of a less accurate modelling of the wall region. The high-frequency (in comparison to the rotational frequency) oscillations of the forces on the airfoil are caused by the shedding of strong vortices resulting from the large separation of the flow during dynamic stall.

The numerical work proves the usefulness of velocity/ vorticity data (in this case, acquired with PIV) for validation. The visualization of the shedding and convection of the vorticity (in particular the location of the leading edge vorticity and the moment of roll-up of the trailing-edge vorticity) proves to be more specific for validation than the comparison of the force on the blade. Simulations with varying grid refinement presented different behaviors of the flow field, specially in terms of the phase at which rollup of the wake of the airfoil occurs; this is clearly identify- able in comparison with experimental vorticity data.

Chapter 7

Environmental Impacts of Wind Energy Farms

7.1 Impacts on human health and well-being

Wind-energy projects can have positive as well as negative impacts on human health and well-being. The positive impacts accrue mainly through improvements in air quality.

In contrast, to the extent that wind-energy projects create negative impacts on human health and well-being, the impacts are experienced mainly by people living near wind turbines who are affected by noise and shadow flicker

7.2 Noise

As with any machine involving moving parts, wind turbines generate noise during operation. Noise from wind turbines arises mainly from two sources: (1) mechanical noise caused by the gearbox and generator; and (2) aerodynamic noise caused by interaction of the turbine blades with the wind. As described below (see “Noise Levels”), noise of greatest concern can be generally classified as being of one of these three types: broadband, tonal, and low-frequency.

The perception of noise depends in part on the individual—on a person’s hearing acuity and upon his or her subjective tolerance for or dislike of a particular type of noise. For example, a persistent “whoosh” might be a soothing sound to some people even as it annoys others. Nevertheless, it appears that subjective impressions of the noise from wind turbines are not totally idiosyncratic. included a laboratory technique for assessing the subjective unpleasantness of wind-turbine noise. Preliminary findings indicated that noise tonality and noise-fluctuation strength were the parameters best correlated with unpleasantness

Broadband, tonal, and low-frequency noise have all been addressed to some degree in modern upwind horizontal wind turbines, and turbine technologies continue to improve in this regard. With regard to the design of a wind-energy project, one is generally interested in assessing whether the additional noise generated by the wind turbines (relative to the ambient noise) might cause annoyance or a hazard to human health and well-being.

Noise impacts also can result from project construction and maintenance. These are generally of relatively short duration and occurrence but can include equipment operation, blasting, and noise

associated with traffic into and out of the facility. These are not addressed in detail in this section. In the following, a brief review of wind-turbine noise and its impacts is presented along with suggested methods for assessing such impacts and mitigation measures.

7.2.1 Noise levels

Noise from wind turbines, at the location of a receptor, is described in terms of sound pressure levels (relative to a reference value, typically 2×10^{-5} Pa) and is typically expressed in dB(A), decibels corrected or A-weighted for sensitivity of the human ear. Note that there is a difference between sound *power* used to describe the source of sound and sound *pressure* used to describe the effect on a receptor. The sound power level from a single turbine is usually around 90-105 dB(A); such a turbine creates a sound pressure of 50-60 dB(A) at a distance of 40 meters (this is about the same level as conversational speech). Noise (sound-pressure) levels from an onshore wind project are typically in the 35-45 dB(A) range at a distance of about 300 meters (BWEA 2000; Burton et al. 2001). These are relatively low noise or sound-pressure levels compared with other common sources such as a busy office (~60 dB (A)), and with nighttime ambient noise levels in the countryside (~20-40 dB(A)). While turbine noise increases with wind speed, ambient noises—for example, due to the rustling of tree leaves— increase at a higher rate and can mask the turbine noise (BLM 2005a).

In addition to the amplitude of the noise emitted from turbines, its frequency content is also important, as human perception of sounds is different at different frequencies. Broadband noise from a wind turbine typically is a “swishing” or “whooshing” sound resulting from a continuous distribution of sound pressures with frequencies above 100 Hz. Tonal noise typically is a “hum” or “pitch” occurring at distinct frequencies. Low-frequency noise (with frequencies below 100 Hz) includes “infrasound,” which is inaudible or barely audible sound at frequencies below 20 Hz.

With older downwind turbines, some infrasound also is emitted each time a rotor blade interacts with the disturbed wind behind the tower, but it is believed that the energy at these low frequencies is insufficient to pose a health hazard (BWEA 2005). Nevertheless, a recent study by van den Berg (2004, 2006) suggests that, especially at night during stable atmospheric conditions, low-frequency modulation (at around 4 Hz) of higher frequency swishing sounds is possible. Note that this is not infrasound, but van den Berg (2006) states that it is not known to what degree this modulated fluctuating sound causes annoyance and deterioration in sleep quality to people living nearby.

Low-frequency vibration and its effects on humans are not well understood. Sensitivity to such vibration resulting from wind-turbine noise is highly variable among humans. Although there are opposing views on the subject, it has recently been stated (Pierpont 2006) that “some people feel disturbing amounts of vibration or pulsation from wind turbines, and can count in their bodies, especially their chests, the beats of the blades passing the towers, even when they can’t hear or see them.” More needs to be understood regarding the effects of low-frequency noise on humans.

7.2.2 Mitigation measures

Noise produced by wind turbines generally is not a major concern for humans beyond a half-mile or so because various measures to reduce noise have been implemented in the design of modern turbines. The mechanical sound emanating from rotating machinery can be controlled by sound-isolating techniques. Furthermore, different types of wind turbines have different noise characteristics. As mentioned earlier, modern upwind turbines are less noisy than downwind turbines. Variable-speed turbines (where rotor speeds are lower at low wind speeds) create less noise at lower wind speeds when ambient noise is also low, compared with constant-speed turbines. Direct-drive machines, which have no gearbox or high-speed mechanical components, are much quieter.

Acceptability standards for noise vary by nation, state, and locality. They can also vary depending on time of day—nighttime standards are generally stricter. In the United States, the U.S. Environmental Protection Agency only provides noise guidelines. Many state governments issue their own regulations (e.g., Oregon Department of Environmental Quality 2006), and local governments often enact noise ordinances. Standards of acceptability need to be understood in the context of ambient (background) noise resulting from all other nearby and distant sources.

7.3 Shadow flicker

As the blades of a wind turbine rotate in sunny conditions, they cast moving shadows on the ground resulting in alternating changes in light intensity. This phenomenon is termed shadow flicker. Shadow flicker is different from a related strobe-like phenomenon that is caused by intermittent chopping of the sunlight behind the rotating blades. Shadow flicker intensity is defined as the difference or variation in brightness at a given location in the presence and absence of a shadow. Shadow flicker can be a nuisance to nearby humans, and its effects need to be considered during the design of a wind-energy project.

In the United States, shadow flicker has not been identified as causing even a mild annoyance. In Northern Europe, on the other hand, because of the higher latitude and the lower angle of the sun, especially in winter, shadow flicker can be a problem of concern.

7.3.1 Impacts

Shadow flicker can be a nuisance to people living near a wind-energy project. It is sometimes difficult to work in a dwelling if there is shadow flicker on a window. In addition to its intensity, the frequency of the shadow flicker is of importance. Flicker frequency due to a turbine is on the order of the rotor frequency (i.e., 0.6-1.0 Hz), which is harmless to humans. According to the Epilepsy Foundation, only frequencies above 10 Hz are likely to cause epileptic seizures. (For reference, frequencies of strobe lights used in discotheques are higher than 3 Hz but lower than 10 Hz.) If a turbine is close to a highway, the movement of the large rotor blades and possible resulting flicker can distract drivers. Irish guidelines, for example, recommend that turbines be set back from the road at least 300 meters (MSU 2004).

7.3.2 Mitigation measures

Shadow flicker is not explicitly regulated. When a maximum number of hours of allowed shadow flicker per year is imposed for a neighbor's property (such as 30 hours/year for one wind-energy project in Germany), this number refers to those hours when the property is actually used by the people there and when they are awake. Denmark has no legislation regarding shadow flicker, but it is generally recommended that there be no more than 10 hours per year when flicker is experienced.

Even in the worst situations, shadow flicker only lasts for a short time each day—rarely more than half an hour. Moreover, flicker is observed only for a few weeks in the winter season. To avoid even limited periods of shadow flicker, a possible solution is to not run the turbines during this time. Obviously, another solution is to site the turbines such that their shadow paths avoid nearby residences.

Since tools for estimation of shadow flicker are readily available, such calculations are routinely done while planning a wind-energy project. One such study was performed for the Wild Horse project in the state of Washington (Nielsen 2003). Using results presented in the form of shadow flicker maps and distributions, one can determine suitable locations for wind turbines. Recently, tools have become available (GH Wind-Farmer) that not only compute shadow flicker in real time during turbine operation, but also convey information to the turbine control system to enable shutdown if the shadow flicker at a particular location becomes particularly problematic. However, the committee is unaware if such real-time systems have been implemented at any specific wind-energy project

7.4 Wind turbines and bird populations

Flying birds sometimes run into buildings and other permanent structures. Wind turbines, however, do not cause a particular problem as has been demonstrated by studies done in other European countries, such as Germany, the Netherlands, Denmark and England. Specifically, it was calculated that out of the total number of birds killed in a year, only 20 deaths were due to wind turbines (for an installed capacity of 1000MW), while 1500 deaths were caused by hunters and 2000 caused by collisions with vehicles and electricity transmission lines (they are almost “invisible” for birds).

7.5 Can wind turbines interfere with television reception?

Wind turbines could, potentially, interfere with television reception in a similar way to any other structure such as electricity pylons, silos and buildings. In the case of wind turbines there is the additional

consideration of the rotation of the blades. In practice this has not proved to be a significant problem, partly because the investigations of any potential wind farm site should include an assessment of the effect on the broadcast reception of local people. Remedial measures are available and developers make provision for taking suitable remedial action if required.

7.6 What happens when a turbine finishes its life?

Wind turbines are typically designed to last for over 20 years. Some replacement of parts might be needed in this period, but the main structure is likely to be in place for at least that long. No wind farm in the UK has yet served its full life and only one has been decommissioned (for economic reasons it was replaced with larger turbines). Some experimental turbines have been taken down.

When a wind farm is decommissioned it is likely that the turbines will be replaced (subject to planning approval) or the structures removed (removal is often a condition of planning consent). Generally all visible traces of the wind farm are removed: the turbines themselves, as well as electrical equipment and roads are all taken away. It is also possible to remove the turbine foundations but sometimes these are left in situ as digging them up would cause greater environmental damage than leaving them.

Summing up, it is important to understand that whatever impacts wind turbines have, on the one hand they are very obvious, and on the other, it is possible to minimize them through proper design and planning. In contrast, the impacts of thermal or nuclear energy production are slow to appear, are long term and no matter how much effort and money are spent, it is impossible to minimize them. In conclusion, we must decide that if we have to produce electricity, it is certainly preferable to produce it in a way which has the smallest possible impact on the environment. From a technical and economic standpoint, the most mature form of renewable and “clean” energy is wind energy. It can effectively contribute to combating climate change while at the same time providing various environmental, social and economic benefits.

Chapter 8

Onshore and Offshore Wind Farms Relative Comparison

8.1 Onshore v-s offshore wind turbines

Onshore wind farms are often subject to restrictions and objections: objections based on their negative visual impact or noise. Restrictions associated with obstructions (buildings, mountains, etc.), land-use disputes or limited availability of lands. These reasons may explain part of the growing importance of offshore systems, but part of the explanation concerns genuine advantages of the offshore turbines, namely higher and more constant wind speeds and, consequently, higher efficiencies.

However, onshore wind systems may also have some advantages over offshore wind farms:

- Cheaper foundation
- Cheaper integration with electrical – grid network
- Cheaper installation and access - during the construction phase
- Cheaper and easier access for operation and maintenance

Besides, small and mini wind turbines (which are necessarily onshore applications) cover a set of needs and goals that offshore wind farms can't.

8.2 Onshore

Onshore turbine installations in hilly or mountainous regions tend to be on ridgelines generally three kilometers or more inland from the nearest shoreline. This is done to exploit the so-called topographic acceleration as the wind accelerates over a ridge. The additional wind speeds gained in this way make a significant difference to the amount of energy that is produced. Great attention must be paid to the exact positions of the turbines (a process known as micro-siting) because a difference of 30 m can sometimes mean a doubling in output.

8.3 Offshore

Offshore wind development zones are generally considered to be ten kilometers or more from land. Offshore wind turbines are less obtrusive than turbines on land, as their apparent size and noise is mitigated by distance. Because water has less surface roughness than land (especially deeper water), the average wind speed is usually considerably higher over open water. Capacity factors (utilisation rates) are considerably higher than for onshore and near-shore locations.

Transporting large wind turbine components (tower sections, nacelles, and blades) is much easier over water than on land, because ships and barges can handle large loads more easily than

trucks/lorries or trains. On land, large goods vehicles must negotiate bends on roadways, which fixes the maximum length of a wind turbine blade that can move from point to point on the road network; no such limitation exists for transport on open water.

Offshore wind turbines will probably continue to be the largest turbines in operation, since the high fixed costs of the installation are spread over more energy production, reducing the average cost. Turbine components (rotor blades, tower sections) can be transported by barge, making large parts easier to transport offshore than on land, where turn clearances and underpass clearances of available roads limit the size of turbine components that can be moved by truck. Similarly, large construction cranes are difficult to move to remote wind farms on land, but crane vessels easily move over water. Offshore wind farms can be large. The Horns Rev array has 80 turbines and as of September 2010, the Thanet Wind Farm is the world's largest off-shore installation with 100 turbines.

8.4 Typical support structures of offshore wind turbines

Support structures for offshore wind towers can be categorized by their configuration and method of installation as described below. These foundations and associated water depths.

8.4.1 Gravity structures.

These foundations resist the overturning loads solely by means of their own gravity. They are typically used at sites where installation of piles in the underlying seabed is difficult, such as on a hard rock ledge or on competent soil sites in relatively shallow waters. Gravity caissons are typically concrete shell structures. These structures are competitive when the environmental loads are relatively low and the dead load is significant, or when additional ballast can be provided at a reasonable cost.

8.4.2 Monopile.

This is a simple design in which the wind tower, made of steel pipe, is supported by the monopile either directly or through a transition piece. The monopile consists of a steel pipe pile up to 6 m (20 feet) in diameter with wall thicknesses as much as 150 mm (6 inches). Depending on the subsurface conditions, the pile is typically driven into the seabed by either large impact or vibratory hammers, or the piles are grouted into sockets drilled into rock. Compared to the gravity base foundation, the monopile has minimal and localized environmental impact. By far, the monopile is the most commonly used foundation for offshore wind turbines.

8.4.3 Guyed monopile towers.

The limitation of excessive deflection of a monopile in deeper waters is overcome by tying the monopile with tensioned guy wires.

8.4.4 Tripods

Where guyed towers are not feasible, tripods can be used to limit the deflections of the wind towers. The pre-fabricated frame is triangular in plan view and consists of steel pipe members connecting each corner. A jacket leg installed at each corner is diagonally and horizontally braced to a transition piece in the center. The tripod braced frame and the piles are constructed onshore and transported by barge to the site. These foundations do not require any seabed preparation.

8.4.5 Braced lattice frame.

A modification of the tripod frame, the lattice frame has more structural members. The jacket consists of a 3-leg or 4-leg structure made of steel pipe that is interconnected with bracing to provide the required stiffness.

8.4.6 Suction buckets.

This design consists of a center column connected to a steel bucket through Flange - reinforced shear panels that distribute the loads from the center of the column to the edge of the bucket. The steel bucket consists of a steel skirt extending down from a horizontal base resting on the soil surface. The bucket is installed by means of suction and behaves as a gravity foundation, relying on the weight of the soil encased by the steel bucket

8.5 Typical foundations

Foundations anchor the support structures to the seabed, and typically fall into the six types described below.

8.5.1 Gravity caissons.

This type of foundation has been used for several offshore wind farms in Europe. For economical fabrication of gravity caissons one requires a shipyard or a dry dock near the site so the massive foundation structures can be floated out to the site and sunk. Site preparation and placement required for gravity caissons typically involves dredging several meters of generally loose, soft seabed sediment and replacing it with compacted, crushed stone in a level bed. Special screeds and accurate surveying is required for this task.

8.5.2 Driven pipe pile.

The driven steel pipe pile option is an efficient foundation solution in deep waters. The typical method of offshore and near-shore installation of piled structures is to float the structure (monopile, tripod or braced frame) into position and then to drive the piles into the seabed using hydraulic hammers. The handling of the piles requires the use of a crane of sufficient capacity, preferably a floating crane vessel. Use of open-ended driven pipe piles allows the sea bottom sediment to be encased inside the pipe, thus minimizing disturbance. The noise generated during pile driving in the marine environment might cause a short-term adverse impact to aquatic life, however, but because the number of piles is typically small, these adverse impacts are only short-term and relatively minor.

8.5.3 Post-grouted closed-end pile in predrilled hole.

A closed-ended steel pipe pile is placed into a predrilled hole and then grouted in place. This option is used often for offshore pile foundations less than 5 m in diameter and offers significant advantages over the cast-in-place drilled shaft option, including advance fabrication of the pile, better quality control, and much shorter construction time on the water. This option requires a specially fabricated large diameter reverse circulation drill. It also requires handling and placement of a long, large-diameter pile, of considerable weight. Closed-end piles can be floated to the site and lowered into the drill hole by slowly filling them with water.

8.5.4 Drilled shafts or bored, cast-in-place concrete pile

. The installation of bored, cast-in-place concrete pile requires driving a relatively thin-walled (25 mm) casing through the soft sediment to the underlying denser material (if necessary to establish a seal), then drilling through and below the casing to the required base elevation. Bending resistance is provided by a heavy reinforcing cage utilizing high strength, large diameter bars, with double ring, where necessary. The casing provides excavation support, guides the drilling tool, contains the fluid concrete, and serves as sacrificial corrosion protection. This approach requires a large, specially fabricated reverse circulation drill.

8.5.5 Composite “drive-drill-drive” pile.

This procedure requires an adaptation of existing drilling and piling techniques and involves a combination of drive-drill-drive sequence to achieve the design depth.

8.5.6 Suction caissons.

Like piles, suction caissons are cylindrical in shape but have larger diameters (10 m to 20 m) and subsequently shallower penetration depths. These caissons are closed at the top. They are installed by sinking into the seabed and then pumping the water out of the pile using a submersible pump. Pumping the water creates a pressure difference across the sealed top, resulting in a downward push that pushes the pile to the design depth. Once the design depth is achieved,

the pumps are disconnected and retrieved. Suction caissons are expected to be particularly suitable for foundations in the type of soft cohesive sediments found around the U.S. coasts. These foundations cannot be used in rock, in gravel or in dense sand. Suction caissons are less expensive to install because they do not require underwater pile drivers. At the end of a wind turbines life, a suction caisson can be removed completely from the seabed, unlike piled foundations. This provides room for recycling.

8.6 Conclusions

The increasing windmill tower and turbine sizes and installations in deeper waters have clearly demonstrated a need for more innovative and cost-effective foundations. There is room for improvement in all areas; in design, through the innovative use of composite materials, support structures and foundations; and in construction processes, through improvements in drilling techniques, fabrication, and transportation. The need for high-capacity foundations that can be installed in deep water with limited accessibility and with little disturbance to the existing environment can also be fulfilled by new technologies and process improvements. Environmental impact can be mitigated by the use of geotextiles for scour protection, and the use of a bubble curtain for noise mitigation.

REFERENCES

1 WIND ENERGY

Wind Energy (2009)

Published online. DOI: 10.1002/we.363

RESEARCH ARTICLE

Simulating Feedback Linearization control of wind turbines using high-order models

A. Kumar and K. Stol

Department of Mechanical Engineering, University of Auckland, Private Bag 92019, Auckland 1142, New Zealand

2 WIND ENERGY

Wind Energy. 2007; **10**:293–301

Published online 7 March 2007 in Wiley Interscience

(www.interscience.wiley.com) DOI: 10.1002/we.221

Influence of Rotor Structural Dynamics Representations on the Electrical Transient Performance of FSIG and DFIG Wind Turbines

Gnanasambandapillai Ramtharan* and Nicholas Jenkins, The University of Manchester, UK

Olimpo Anaya-Lara, University of Strathclyde, UK

Ervin Bossanyi, Garrad Hassan & Partners Ltd, UK

3 INTERNATIONAL JOURNAL OF ENERGY RESEARCH

Int. J. Energy Res. 2000; 24: 77–92

systems with double output induction generator

Sliding mode control for efficiency optimization of wind energy

P. F. Puleston*, R. J. Mantz, P. E. Battaiotto and F. Valenciaga

LEICI, Electrical Engineering Department, University of La Plata, C.C. 91, La Plata C.P. 1900,

Argentina

4 Electrical Engineering in Japan, Vol. 150, No. 4, 2005

Translated from *Denki Gakkai Ronbunshi*, Vol. 124-B, No. 2, February 2004, pp. 259–266

Turbine-Generator Systems

TETSUYA WAKUI,¹ YOSHIAKI TANZAWA,² TAKUMI HASHIZUME,¹ and TOSHIO NAGAO³

¹Waseda University, Japan

2Nippon Institute of Technology, Japan
3E&E Co., Japan

22. Bourisand D, Bergeles G. 2D LES of vortex shedding from a square cylinder. *Journal of Wind Engineering and Industrial Aerodynamics* 1999; **80**: 31–46
March.

23. Shao J, Zhang C. Numerical analysis of the flow around a circular cylinder using RANS and LES. *International Journal of Computational Fluid Dynamics* 2006; **20**: 301–307.

17. Fluent User's Manual. Fluent, Inc.: Digital edition.

18. Spalart PR, Almaras S. A one-equation turbulence

7. Simão Ferreira CJ, van Bussel G, van Kuik G, Scarano F. Visualization by PIV of dynamic stall on a vertical axis wind turbine. *Experiments in Fluids* 2009; **46**: 97–108.

10. Hansen MOL, Sørensen DN. CFD model for vertical axis wind turbine. *Wind Energy for the New Millennium—Proceedings of the European Wind Energy Conference, Copenhagen, 2001*; 485–488.

11. Allet A, Hallé S, Paraschivoiu I. Numerical simulation of dynamic stall around an airfoil in Darrieus motion. *Journal of Solar Energy Engineering* 1999; **121**: 69–76.

12. Paraschivoiu I, Allet A. Aerodynamic analysis of the Darrieus wind turbines including dynamic-stall effects. *Journal of Propulsion and Power* 1988; **4**: 472–477.

13. Paraschivoiu I, Béguier C. Visualization, measurements and calculations of dynamic stall for a similar

Ermiş M. *et al.* 1992. Various induction generator schemes for wind electricity generation. *Electric Power Systems Research* 23:71–83.

Salameh Z, Kazda L. 1986. Analysis of the steady state performance of the double output induction generator *IEEE Transaction on Energy Conversion* 1(1):26–32

. Salameh Z, Kazda L. 1986. Analysis of the steady state performance of the double output induction generator *IEEE Transaction on Energy Conversion* 1(1):26–32.

10. Hansen MOL, Sørensen DN. CFD model for vertical

axis wind turbine.

Millennium—Proceedings of the European Wind Energy Conference, Copenhagen, 2001; 485–488.

11. Allet A, Hallé S, Paraschivoiu I. Numerical simulation of dynamic stall around an airfoil in Darrieus motion. *Journal of Solar Energy Engineering* 1999; **121**: 69–76.

12. Paraschivoiu I, Allet A. Aerodynamic analysis of the Darrieus wind turbines including dynamic-stall effects. *Journal of Propulsion and Power* 1988; **4**: 472–477.

13. Paraschivoiu I, Béguier C. Visualization, measurements and calculations of dynamic stall for a similar motion of VAWT. *Proceedings of the European Wind Energy Conference, Herning, 1988; 197–202.*